NICKEL ALUMINATE SPINEL-DERIVED CATALYSTS FOR THE AQUEOUS PHASE REFORMING OF GLYCEROL: EFFECT OF REDUCTION TEMPERATURE

A. Morales-Marín[1], J.L. Ayastuy[1,*], U. Iriarte-Velasco[2], M.A. Gutiérrez-Ortiz[1]

Applied Catalysis B: Environmental 244 (2019) 931–945

DOI: 10.1016/j.apcatb.2018.12.020

NICKEL ALUMINATE SPINEL-DERIVED CATALYSTS FOR THE AQUEOUS PHASE REFORMING OF GLYCEROL: EFFECT OF REDUCTION TEMPERATURE

A. Morales-Marín[1], J.L. Ayastuy[1,]*, U. Iriarte-Velasco[2], M.A. Gutiérrez-Ortiz[1]

Chemical Technologies for the Environmental Sustainability Group,

[1]Department of Chemical Engineering, Faculty of Science and Technology

University of the Basque Country UPV/EHU,

Sarriena S/N, 48940 Leioa, Spain

[2]Department of Chemical Engineering, Faculty of Pharmacy

University of the Basque Country UPV/EHU,

Paseo de la Universidad, 7, 01006 Vitoria, Spain

**Corresponding author*: joseluis.ayastuy@ehu.eus

Keywords: Nickel; spinel; aqueous phase reforming; glycerol; hydrogen

Abstract

Bulk nickel aluminate ($NiAl_2O_4$) was synthesised by co-precipitation at a Ni/Al mole ratio of 1:2 (stoichiometric ratio). The prepared sample was reduced at different temperatures, in the 300 to 850 ºC range, and obtained assays were analysed by a wide range of analytical techniques (XFR, XRD, H_2-chemisoprtion, H_2-TPR, DRS UV-vis NIR, FTIR, ^{27}Al MAS NMR, NH_3-TPD, CO_2-TPD, TPO) and tested for the APR of glycerol. The spinel precursor allowed the formation of small and stable Ni particles (< 14 nm) upon reduction with good performance in the APR of glycerol (NiAl-850 93% conversion, 57% conversion to gas, at 250 ºC/45 bar and WHSV 24.5 h^{-1}). Hydrogen was the main gaseous product and the activation temperature did not substantially alter selectivity to gaseous products; however, selectivity to intermediate oxygenated liquid compounds was substantially modified. Overall, glycerol dehydrogenation route was dominant at high reduction temperature. The good stability of the spinel led to stable H_2 yield in the long-term runs (50 hours) and proved potential to be used in the APR of glycerol.

1. Introduction

Glycerol (1,2,3-propanetriol) is a major by-product during the production of biodiesel by transesterification of vegetable oils [1], animal fats [2] and waste oils [3]. Glycerol is generated at approximately 10 wt.% of the total biodiesel produced. Thus, the huge increase in the worldwide production of biodiesel [4] leads to a large amount of glycerol surplus, which must be recycled into higher value-added chemicals for the economic viability of biodiesel industries. The high functionalization of the glycerol molecule makes it prone to many different processes such as oxidation, hydrogenolysis and dehydration [5].

Glycerol can be also used as hydrogen source, as alternative to the traditionally used catalytic steam reforming of methane [6]. The catalytic aqueous phase reforming (APR) of biomass-derived oxygenated hydrocarbons was introduced by first in 2002 by the group of Dumesic [7]. The process can be carried out at relatively low temperatures (200-280 ºC) and moderate pressures (15-70 bar) as compared to gas-phase reforming and the selection of proper operation conditions, feedstreams and catalysts can be used to drive the APR to either hydrogen or alkanes production [8]. Thus, undesirable decomposition reactions, such as coke deposition, can be minimized whereas H_2 production can be increased by the Water-Gas Shift reaction (WGS) [6]. APR is also energy-efficient since water and glycerol are not vaporized. Moreover, the concentration of glycerol among the byproducts of biodiesel is optimal to the APR, therefore no pre-treatment is required in order to adjust water/glycerol ratio.

The ideal APR of glycerol yields seven moles of hydrogen and three moles of CO_2 per mole of glycerol (Eqs. 1-3):

$$C_3H_8O_3\ (l) \rightarrow 3CO + 4H_2 \qquad \Delta H^0 = +338.0\ kJ/mol \qquad (1)$$

$$CO + H_2O \leftrightarrows CO_2 + H_2 \qquad \Delta H^0 = +3.38\ kJ/mol \qquad (2)$$

$$C_3H_8O_3\ (l) + 3H_2O \rightarrow 7H_2 + 3CO_2 \qquad \Delta H^0 = +348.1\ kJ/mol \qquad (3)$$

A catalyst with high H_2 selectivity must promote C-C and C-H bond cleavage and WGS reaction, and should minimize the C-O cleavage (i.e. CO and CO_2 hydrogenation) [9]. Platinum, ruthenium and in general, metals from Group VIII exhibit high APR activity [10-12]. Benchmark supported platinum catalysts are recognized as the most active and selective catalysts due to their moderate activity in C-C and C-H bond cleavage [6] and low methanation and Fisher-Tropsch activity [8]. In the recent years, nickel based catalysts have attracted considerable attention for the APR process as due to economic criteria as well as its good intrinsic activity in C-C scission, especially high by small particles [11,13-16]. Nickel supported on conventional γ-alumina has been extensively investigated because of adequate textural properties. However, under APR hydrothermal conditions, γ-Al_2O_3 can

be hydrated and transformed into boehmite (γ-AlOOH), with significant alteration of its surface area and acidity. This may provoke activity decay [17] due to dissolution of the support and sinterisation of metal particles [18].

The nature of oxide surfaces that support the metal phase are of critical importance [19,20]. Nickel aluminate ($NiAl_2O_4$) spinels are known to present a partially inverted structure with part of Ni^{2+} ions occupying octahedral sites and part of Al^{3+} ions tetrahedral ones [21]. On the other hand, the inversion degree of spinels notably affects the nature of the surfaces and also their catalytic properties [22]. The reduction step, indeed, can alter the structural properties. Thus, if metal-support interaction is improved, a better catalytic behaviour could be obtained [23].

In the reduction process of spinel, the oxygen vacancies move through the spinel to the particle surface. As a consequence, changes in the surface microstructure occur, with a major fraction of the nickel metal particles forming on the surface. This way the creation of a nickel aluminate layer between the metallic nickel particles and the alumina could prevent sintering [19]. It has been reported that reduction at high temperatures promotes the rearrangement of nickel in the aluminate matrix, and relatively small Ni crystallites with good textural stability can be obtained [23] what would imply a significant advantage for catalytic applications. It has been reported that reduction of the nickel aluminate leads to metallic Ni in strong interaction with alumina [24].

In this work nickel aluminate spinel was synthesized by coprecipitation at a stoichiometric nickel to alumina mole ratio. It was activated at different reduction temperatures and the catalytic behaviour in glycerol aqueous phase reforming was evaluated. Catalysts characterization was carried out by a wide number of techniques (XRD, UV–visible–NIR DRS, FTIR, ^{27}Al MAS NMR, H_2-TPR, H_2-chemisorption, CO_2-TPD, NH_3-TPD and TPO) and related to the catalytic performance. Adequate nickel speciation and nickel-support interactions were sought in order to attain high selectivity to hydrogen. To the best of our knowledge, the properties and the application of this catalytic system for the glycerol aqueous phase reforming have not been yet investigated.

2. Experimental

2.1. Catalysts preparation

Bulk nickel aluminate ($NiAl_2O_4$) was synthesised by co-precipitation at a Ni/Al mole ratio of 1:2 (stoichiometric ratio). The procedure was as follows: proper amounts of nickel acetate (99.998% trace metals basis, Sigma-Aldrich) and aluminium nitrate (98.0% purity, Fluka) aqueous solutions were mixed in a vessel at ambient temperature. Aqueous ammonia was added to adjust pH at 8. Solution was continuously stirred for 30 min, while the precipitated was formed. The suspension was kept at ambient temperature for 30 min. The as-prepared solid was filtered, washed thoroughly with distilled

81 water at 90 ºC, dried overnight at 110 ºC and then calcined at 850 ºC (heating rate 10 ºC/min, hold 4
82 h). The as-prepared precursor was divided into six parts. Five were reduced at different temperatures
83 (300, 450, 600, 700 and 850 ºC) and remaining part was no further modified. For the characterization
84 where in-situ reduction was not possible, the reduction was carried out ex-situ, in a quartz reactor,
85 under 5%H_2/He flow of 50 mL/min (heating at 10 ºC/min, hold 1 h) from room temperature to the
86 desired temperature. Finally, sample was cooled down to room temperature in 5%H_2/He flow. The
87 reduced samples were labeled as NiAl-T, where T indicates the reduction temperature. The unreduced
88 sample was labeled as NiAl-c. Spent catalysts were named as NiAl-T-u (used for 2 h) or NiAl-T-50h
89 (after 50 h TOS). For comparative purposes, γ-alumina and NiO were also prepared by simple
90 calcination in air (at 850 ºC) of aluminium nitrate and nickel acetate, respectively.

91 2.2. Characterization techniques

92 Bulk composition was determined by XRF (AXIOS, PANalytical), by using the fusion method. The
93 amount of leached metals was measured by ICP-AES in the overall liquid sample collected after each
94 reaction. The textural properties were obtained from the nitrogen adsorption-desorption isotherms
95 determined at 77 K in Micromeritics TRISTAR II 3020 equipment. Previously, each sample was
96 outgassed at 300 ºC for 10 h, in order to remove moisture and carbon dioxide. The specific surface
97 area and the pore size distribution were determined by the BET and BJH methods, respectively.

98 The identification of crystalline phases and the morphological study was carried out by X-ray
99 diffraction conducted on a PANalytical Xpert PRO X-ray diffractometer with Cu Kα radiation (λ =
100 1.5418 Å). Scattered radiation was measured in the range 2θ = 10-80°, with step size 0.026° and a
101 counting time of 2.5 s/step. The crystallite size of each species was estimated from its most intense
102 peak, by using the Scherrer equation. Crystalline phases present in the samples were identified by
103 comparing with the ICDD database.

104 Exposed metallic Ni atoms per catalyst gram and the Ni metallic surface area were calculated from
105 H_2 chemisorption, carried out in a Micromeritics AutoChem 2920 equipment. Prior to analysis, the
106 samples were heated in He stream at 100 ºC, and then reduced under 5% H_2/Ar flow for 2 h at the
107 corresponding reduction temperature. Then the sample was cooled down to 35 ºC under Ar flow.
108 Then, H_2 pulses (loop volume 0.5312 mL) were injected until saturation. The exposed metal surface
109 area was calculated assuming H:Ni stoichiometry of 1:1 [25] and spherical Ni particles, with cross-
110 sectional area of 0.065 nm^2 and density of 8.9 cm^3/g [26].

111 The reducibility of the prepared samples was studied by temperature-programmed reduction (H_2-
112 TPR) in a Micromeritics AutoChem 2920 instrument. For NiAl-c, about 70 mg of sample was initially
113 flushed in 5% O_2-He stream at 550 °C for 1 h (heated at 10 °C/ min). It was cooled down to room

temperature in Ar flow. Then, a flow of 5% H_2-Ar was passed through the bed containing the sample while temperature was increased to 950 ºC at 10 ºC/min, and hold for 1 h. The H_2 consumption rate was monitored in a previously calibrated thermal conductivity detector (TCD). The total H_2 consumption measured for sample NiAl-c was defined as TPR-a.

Also, H_2-TPR was carried out for the partially reduced samples (NiAl-T) in order to calculate the fraction of reduced nickel ($f_{Ni,red}$). Firstly, approximately 70 mg of each sample was reduced at temperature T, following the same protocol as for TPR-a. The amount of H_2 consumed in this stage was defined as TPR-b. Then, it was cooled down to room temperature in He flow, and subsequent TPR run, up to 950 ºC, was carried out. The amount of H_2 consumed in this stage was defined as TPR-c. The value $f_{Ni,red}$ for each NiAl-T sample was defined as the fraction of the amount of H_2 consumed during its reduction at temperature T (TPR-b) with respect to the total amount of H_2 consumed during the reduction of NiAl-c (TPR-a).

The speciation of nickel cations (coordination and oxidation states) was analysed by Diffuse Reflectance UV-vis spectroscopy with a UV-vis-NIR Cary 5000 equipment coupled to Diffuse Reflectance Internal 2500 within the range 200-2500 nm. Kubelka–Munk function was applied to convert the DRS into equivalent absorption.

Fourier transform infrared spectroscopy (FTIR) transmittance spectra were recorded in the 400-4000 cm^{-1} range in a Cary 600 Series FTIR apparatus by employing KBr pellet technique, as an average of 50 scans with a resolution of 4 cm^{-1}.

^{27}Al Solid State NMR measurements were performed on a 9.4 T Bruker AVANCE III 400 spectrometer operating at resonance frequencies of 104.26 MHz for 27Al. Chemical shifts were referenced externally to the $AlCl_3$ aqueous solution at 0 ppm. The spectra were acquired at a spinning frequency of 60 kHz employing a PH MASDVT400W BL 1.3mm ultrafast probehead. A single pulse of 0.3 microseconds duration was applied and a recycle delay of 0.2 s and 36,000 scans were used.

Surface acidity and basicity were measured by NH_3 pulse chemisorption and CO_2 temperature programmed desorption, respectively. Measurements were carried out in a Micromeritics AutoChem 2920 instrument coupled to Mass Spectroscopy (MKS, Cirrus 3000). About 35 mg of the calcined precursor was initially pretreated in 5%O_2-He stream at 550 °C for 1 h (heating rate 10 °C/ min) and cooled to room temperature. Then, it was reduced at the desired temperature in 5%H_2/Ar flow (heating rate 10 ºC/min), hold for 1 h and cooled down in He flow (to 90 °C for NH_3 adsorption and to 40 ºC for CO_2 adsorption). For acidity measurements, a series of 10% NH_3-He pulses (loop volume 0.5312 mL) were introduced at 90 ºC until constant peak area was achieved. Then, temperature was raised (10 ºC/min) to 850 ºC into He flow, and the released gases were monitorised by MS (MKS

Cirrus) [27]. For basicity measurements, 5% CO_2/He flow was passed through the sample at 40 °C up to saturation. Subsequently, the sample was exposed to a He flow for 60 min at 40 °C in order to remove reversibly and physically bound CO_2. Finally, the temperature was raised to 900 °C (heating rate 10 °C/min) and the resultant signal was followed by MS.

Carbon deposition on spent catalysts was evaluated by temperature-programmed oxidation (Setaram Setsys evolution) coupled to mass spectroscopy (Pffeifer OmniStar) to follow the evolution of m/z signals 44 (CO_2) and 18 (H_2O). Approximately 5 mg of calcium carbonate (used as reference) was added to about 25 mg of sample. The mixture was treated under 5%O_2/He at 150 ºC for 1 h and then heated up to 1000 ºC at a heating rate of 5 ºC/min.

2.3. Catalytic performance evaluation

The aqueous phase reforming (APR) of glycerol was studied in a bench-scale fixed-bed up-flow reactor (Microactivity Effi, PID Eng&TEch). The reactor (i.d. 5.1 mm, height 305 mm) was made of Hastelloy alloy. In a typical run, about 0.5 g of catalyst (particle size 0.04-0.16 mm) were placed on a stainless steel frit and covered with a quartz wool plug. Prior to reaction, it was reduced "in situ", at atmospheric pressure, under 20% H_2 flow (balance He) to the desired reduction temperature, T (heating rate 5 ºC/min), and hold for 1 h. Then, He flow was switched to bypass and 10 wt.% glycerol (Panreac, >99.5% purity) aqueous solution was pumped into the reactor at 0.2 mL/min. Resultant WHSV (determined as the ratio between feed mass-flowrate and mass of fresh catalyst) was of 24.5 h^{-1}. Catalytic performance was measured after two hours of operation. Three temperature/pressure APR conditions were tested: 235 ºC/35 bar, 250 ºC/45 bar and 260 ºC/52 bar. Reaction products were cooled down to 5 ºC. The gas products were swept with 40 mL/min of He flow introduced immediately before backpressure regulator, and continuously analyzed by a GC-MS (μGC Agilent, equipped with four columns (Al_2O_3-KCl 10 m, PPQ 10 m, MS5A 10 m, He as carrier and MS5A 10 m, Ar as carrier). The liquid products were analyzed off-line by GC-MS (Agilent, CP-Wax 57CB column) and HPLC-RI (Waters, Hi-Plex H column). Total organic carbon (TOC) in the condensable phase was measured on a Shimadzu TOC-5050A apparatus.

The total glycerol conversion (X_{Gly}) was calculated as follows:

$$X_{Gly}(\%) = 100 \times \frac{F^{in}_{Glycerol} - F^{out}_{Glycerol}}{F^{in}_{Glycerol}} \quad (4)$$

The carbon conversion to gas (X_{gas}) was calculated as follows:

$$X_{gas}(\%) = 100 \times \frac{F^{in}_{C_{atoms,feed}} - F^{out}_{C_{atoms,liquid}}}{F^{in}_{C_{atoms}}} \quad (5)$$

Selectivity to gas (S_{gas}) was defined as the fraction of carbon moles converted into gas phase per converted glycerol moles:

$$S_{gas}(\%) = 100 \times \frac{F^{in}_{C_{atoms,feed}} - F^{out}_{C_{atoms,liquid}}}{F^{in}_{Glycerol} - F^{out}_{Glycerol}} \times \frac{1}{3} \quad (6)$$

Hydrogen selectivity (S_{H2}) was defined as the ratio between the moles of hydrogen produced and moles of glycerol reacted, multiplied by 1/7 (inverse of the reforming glycerol/hydrogen ratio, according to reaction (3):

$$S_{H_2}(\%) = 100 \times \frac{F^{out}_{H_2}}{F^{in}_{Glycerol} - F^{out}_{Glycerol}} \times \frac{1}{7} \quad (7)$$

The selectivity of the C-containing product i was calculated as follows:

$$S_i(\%) = 100 \times \frac{F^{out}_{i}}{F^{in}_{Glycerol} - F^{out}_{Glycerol}} \times \frac{C_{atoms,i}}{3} \quad (8)$$

Finally, hydrogen yield (Y_{H2}) was defined as the ratio between the moles of hydrogen produced and moles of glycerol fed into the reactor:

$$Y_{H2}(\%) = 100 \times \frac{F^{out}_{H2}}{F^{in}_{Glycerol}} \times \frac{1}{7} \quad (9)$$

3. Results and discussion

3.1. Materials characterization

3.1.1. Chemical composition and textural properties

The experimentally measured nickel loading was 31.3 wt.%, very close to the stoichiometric value (33.2%). Textural properties, detailed in Table 1, revealed that specific surface area of nickel aluminate NiAl-c was very similar to that of bare alumina (101.6 m^2/g, Table S1, Supporting Information). However, pore volume and average pore size (Table S1, Supporting Information) increased more than two fold after incorporation of Ni. Type IV (IUPAC classification) isotherms (Figure S1A, Supporting Information), characteristic of mesoporous solids, with H_2 hysteresis loop, related to disordered porous materials were observed for the prepared assays, irrespective of the reduction temperature. A slight increase in the pore volume, and average pore size (Table S1, Supporting Information), occurred with increasing the reduction temperature. Concomitantly, surface area slightly decreased (S_{BET} 98.0 m^2/g for NiAl-c; 76.6 m^2/g for NiAl-850), likely due to the phase transformation from $NiAl_2O_4$ to Ni/Al_2O_3 [28,29] and the dilution effect. Also, partial blockage of pores cannot be discarded. Overall, this behaviour pointed to a high structural stability of the stoichiometric $NiAl_2O_4$. Pore size distribution (PSD) showed a unimodal structure for all samples

(Figure S1B, Supporting Information). It was observed that reduction at above 450 ºC shifted PSD to larger values, likely caused by the collapse of the smallest pores.

TABLE 1

3.1.2. H_2-TPR and H_2-chemisorption

The reducibility of the nickel aluminate spinel precursor (NiAl-c) and the partially reduced catalysts (NiAl-T) was studied by temperature programmed reduction (H_2-TPR), and the obtained TPR profiles are shown in Figure 1A. The reduction profile of NiO is also included for comparison. Note that TPR profiles of NiAl-T samples corresponded to the so-called TPR-c, that is, the hydrogen consumption profile of samples previously reduced at temperature T.

FIGURE 1

NiO exhibited a relatively narrow reduction peak in the 240 ºC to 415 ºC range, with its maximum at 377 °C. All Ni was reduced at below 400 ºC as deduced from the experimentally measured hydrogen consumption of 13.4 $mmol_{H2}/g$ (theoretical value 13.3 $mmol_{H2}/g$). Bare γ-Al_2O_3 showed no H_2 consumption in the studied temperature range (not shown). It was clear that incorporation of aluminium significantly modified the reduction profile of NiO. The observed shift in the reduction profile of NiAl-c and that of the partially reduced catalysts evidenced the intimate interaction of Ni with alumina. The left tail suggested the existence of a number of nickel species with different reducibility. The H_2-TPR curve was split into peaks named α, β and γ, for the low, medium and high temperature hydrogen consumption, respectively [30]. The α peak was ascribed to the reduction of easily reducible surface free nickel oxide [30], formed in close interaction with the non-stoichiometric nickel aluminate spinels [31]. The medium temperature β peak was ascribed to Ni^{2+} species in a deffective $Ni_{1-X}Al_2O_{4-X}$ phase [32]. Finally, the high temperature peak (γ), centered at 837 ºC, was related to the reduction of Ni^{2+} species in the $NiAl_2O_4$ spinel lattice [24]. Free nickel oxide (α peak) was reduced around 150 ºC above that of bare NiO, what reflected the strong interaction between NiO particles and the less reducible alumina [33].

Peak β was split into two contributions, namely β_1 (at lower temperature) and β_2 (at higher temperature). The molar ratio β_1/β_2 for the non-reduced sample was 1.10, which, in turn, decreased with the reduction temperature (Table 2). This suggested that composition of defective $Ni_{1-X}Al_2O_{4-X}$ depends upon reduction treatment, likely β_1 referred to Ni-rich solid and β_2 referred to Ni-lean solid [34].

TABLE 2

Hydrogen consumption of β and γ species scarcely varied upon reduction below 450 ºC, causing a relative contribution to overall Ni species of around 45% and 52%, respectively. Reduction at 600 ºC decreased the hydrogen consumption of the defective spinel phase (β peak) to half, and for NiAl-700 sample Ni^{2+} species in the resultant catalyst were mainly as $NiAl_2O_4$. Eventually, at 850 ºC, all Ni added was fully reduced (Table 2, Figure 1A).

It has been suggested that reduction of α-type NiO produced large Ni particles [32,35]. The quantitative results of the TPR profiles (Table 2) showed that α-type species were less than 2% for the catalyst precursor studied here. Thus, the small average crystallite size of Ni^0 particles obtained (Table 1) could be partially attributed to the lack of "free" nickel oxide species and the fact that catalyst precursor contained mainly Ni^{2+} species in spinel-like structure which favored dispersion of the metallic nickel phase formed upon reduction.

Results from hydrogen pulse chemisorption are given in Table 2. As expected, the accessible metallic nickel surface increased with the reduction temperature from 0.07 m^2_{Ni}/g for NiAl-300 to 3.47 m^2_{Ni}/g for NiAl-850 (in terms of exposed Ni atoms it increased from $1.14 \cdot 10^{18}$ for NiAl-300 to $53.4 \cdot 10^{18}$ at_{Ni}/g for NiAl-850), as due to the migration of nickel from spinel phase to the catalyst surface. As shown by TPR, diffusion of Ni^{2+} commenced at around 600 ºC (also discussed in XRD and ^{27}Al NMR sections).

3.1.3. XRD characterization

The most prominent features of XRD patterns are ascribed to cubic spinel structure (JCPDS 78-1601) (Figure 2A). Diffraction line at 2θ=65.6º (plane (440)) confirmed the formation of $NiAl_2O_4$ spinel. NiO was not detected, probably, because of the smaller than detection limit (2-5 nm) size of the crystallites. Characteristic features of metallic nickel appeared upon reduction at 600 ºC or above (2θ = 44.5º, 51.8º and 76.4º) (JCPDS 01-087-0712), and increased in intensity with reduction temperature. It was observed that reduction at ≤ 600 ºC hardly altered the XRD spectra peak shape and position (i.e. 2θ = 19.0, 37.0 and 59.6º remained almost constant) reflecting the high stability of the $NiAl_2O_4$ phase. Although TPR analysis confirmed that about 6% of the nickel in the spinel precursor was reduced at 450 ºC, its absence in the XRD spectra highlighted an adequate dispersion of the metal. The formation of γ-alumina phase (JCPDS 79-1558) could be recognized upon reduction at 850 ºC.

From a structural perspective, the experimentally measured lattice parameter for the unreduced sample was 8.044 Å (Table S2, Supporting Information), very close to that of stoichiometric nickel aluminate spinel (8.0451 Å) [21]. Values of lattice parameter decreased with reduction temperature. This lattice compression reflected the migration of the nickel ions from the nickel aluminate lattice

to the surface, suggesting that the solid bulk was progressively enriched in alumina. Upon reduction, metallic nickel crystallized into *Fm-3m* cubic system (JCPDS 01-087-0712). No evidence was found for hexagonal close packed nickel. At the highest reduction temperature of 850 ºC, 2θ position for plane (440) shifted to 67.3° (given as Δθ in Figure S2, Supporting Information), reinforcing the idea that nickel was drawn towards Ni clusters and matrix composition tended to γ-Al_2O_3 [29].

The intensity ratio of peaks corresponding to (220) and (440) reticular planes (I_{220} / I_{440}) (Table S2, Supporting Information) varied among the prepared catalysts. The intensity ratio I_{220} / I_{440} was related to cation distribution [36]. As the ionic radius of Ni^{2+} cation (0.69 Å) exceeds that of Al^{3+} (0.54 Å), I_{220} / I_{440} increases with increasing Ni^{2+} cations on tetrahedral sites (T_d), and the ratio decreases with increasing occupancy of Ni^{2+} cations on octahedral sites (Oh). For "normal" spinel this ratio would approximate to 0.33. We measured a value of 0.25 for NiAl-c (Table S2, Supporting Information), and a decreasing trend with reduction temperature (i.e. I_{220} / I_{440} = 0.21 for sample NiAl-700) was observed. That is, the reduced system was slightly enriched in Ni^{2+} cations hosted in octahedral sites. Therefore, we might conclude that tetrahedral Ni^{2+} cations were more readily reduced as compared to octahedral Ni^{2+} sites. Presumably, the lattice oxide ions of the trigonal prism stabilize the Ni^{2+} ion rather effectively.

FIGURE 2

Crystallite size of nickel aluminate and metallic nickel (in reduced catalysts) varied in the 9-10 nm and 8-14 nm range, respectively (Table 1). In both cases, no clear trend in crystal growth was observed with the reduction temperature. The relatively small size of the metallic nickel nanoclusters formed in our system, in spite of the high reduction temperature, reflected the strong interaction of nickel with the Ni-Al-O support, which stabilized Ni particles and reduced their surface mobility, protecting against the sinterisation under reductive atmosphere [32,34]. For instance, Ni/alumina catalysts prepared by wet impregnation, and at a similar nickel content, showed a metallic nickel crystallite size of about 26 nm [37].

3.1.4. Skeletal DRS UV-vis NIR and IR characterization

Figure 3 shows the diffuse reflectance UV-vis NIR spectra of the prepared samples. Main features of NiO spectra include the broad bands in the 900-1400 nm and 250-350 nm regions, ascribed to $O^{2-} \rightarrow Ni^{2+}$ charge transfers [38] and $^3A_{2g} \rightarrow {}^3T_{1g}(F)$ transition bands at 377, 414 and at 720 nm. All these features are characteristic of octahedral Ni^{2+} in NiO lattice [39]. For catalyst NiAl-c, the intensity in the $O^{2-} \rightarrow Ni^{2+}$ charge transfers region increased whereas it was attenuated in the visible range, at around 720 nm, what suggested that Ni^{2+} cations existed in a different electronic environment as compared to bare NiO. The intense doublet, with maxima at 605 and 638 nm, observed for catalyst

NiAl-c, was attributed to the $^3T_1 \rightarrow {}^3T_2$ (^3P) spin-allowed transition of Ni^{2+} ions in tetrahedral symmetry (Ni^{2+}_{Td}). Moreover, absorption bands centered at 550 and 760 nm characteristic of Ni^{2+}_{Td} were clearly observed. Thus, these results reflected that Ni^{2+} ions were embedded in the alumina lattice to form $NiAl_2O_4$ phase in the non-reduced NiAl-c sample, in accordance with XRD data.

The DRS UV-vis NIR spectra of partially reduced samples (i.e. ≤ 450 ºC) were qualitatively similar to NiAl-c. Reduction at 600 ºC removed typical features of NiO and nickel aluminate and only some complex bands at around 330 nm were observed, ascribed to metallic nickel nanoparticles [40].

The intensity ratio of the doublet at 600-650 nm to peak at 1100 nm ($Ni^{2+}_{Td}/Ni^{2+}_{Oh}$) was used to measure the relative content of Ni^{2+}_{Td} with respect to Ni^{2+}_{Oh} [41]. The experimentally measured values (Table S2, Supporting Information) reflected that the highest $Ni^{2+}_{Td}/Ni^{2+}_{Oh}$ corresponded to sample NiAl-c, and decreased upon reduction, what supports the XRD data.

FIGURE 3

Further structural characterization carried out by FTIR analysis (Figure S3, Supporting Information) confirmed the above observations. Spinel structure was identified in sample calcined at 850 ºC which was readily transformed into γ-alumina under H_2 flow. In the FTIR spectra, alumina could be detected upon reduction above 600 ºC (Figure S3A, Supporting Information)

3.1.5. ^{27}Al MAS NMR

Figure 4A shows the ^{27}Al MAS NMR spectra of NiAl-T samples. The spectrum of γ-Al_2O_3 consisted of two peaks at 3.7 and 60 ppm (i.e. octahedral and tetrahedral aluminium, respectively), with an intensity ratio of 73:27, as also reported by others [42].

The non-reduced assay showed a broad peak centered at -33 ppm, reflecting the predominant existence of Al_{Oh}. The subtle peak at around 70 ppm denoted the presence of Al_{Td}, characteristic of partially inverted spinels. Reduction at below 600 ºC hardly varied the Al-NMR spectra, and Al^{3+} mainly occupied the octahedral sites. However, reduction at above 600 ºC increased the amount of Al_{Td} in the catalyst, as deduced from the enlarged signal at around 60 ppm. This is consistent with the departure of Ni^{2+} to octahedral sites to ensure neutrality. Indeed, Figure 4B shows that Al_{Oh} chemical shift linearly increased with the reduction temperature, which was bottom and upper limited by NiAl-c (-33.3 ppm) and γ-alumina (+3.8 ppm). For NiAl-850 sample, δ_{AlOh} was +0.8 ppm, close to γ-alumina.

FIGURE 4

3.1.6. Surface acidity and basicity

Aqueous phase reforming of glycerol involves, among others, dehydration reactions [15], which are very sensitive to catalysts surface acid-base properties [43]. Therefore, the study of the total amount and strength of such functionalities could help the interpretation of the activity and selectivity data. Results from CO_2 and NH_3 chemisorption are given in Table 1 and Figure 5.

Activation under hydrogen flow increased acidity, up to 35% (highest value for NiAl-850: 2.13 $\mu mol_{NH3}/m^2$). The increase of surface basicity was even more marked, up to a two-fold increase, especially at the most severe reduction conditions. The fact that strong sites decreased during reduction suggested that exposed coordinatively unsaturated nickel cations and oxygen species in the calcined spinel may act as strong acid and basic sites, respectively. Treatment under hydrogen flow caused surface enrichment in medium strength sites. This was probably due to the progressive dehydroxylation of the surface and increase of exposed γ-alumina on surface, as revealed by XRD, FTIR and ^{27}Al MAS NMR. Actually, reduction at above 600 ºC completely removed strong sites. Moreover, it has been reported that reduced Ni could react with strong acid sites and generate Ni^{2+} ions (as NiO), which increase the middle-strength acidity [44]. The observed complexity in the medium strength desorption region as reduction temperature increased (Figure S4, Supporting Information) could be ascribed to modification of the oxygen coordination in the catalyst surface. Overall, based on the APR selectivity data discussed later, it can be deemed that these differences in the acid-base properties were sufficient to change catalyst performance.

FIGURE 5

3.1.7. General overview of the catalysts physico-chemical properties upon reduction

Nickel species of different reducibility were found in the nearly stoichiometric $NiAl_2O_4$ prepared by coprecipitation: (i) a small fraction of surface free nickel oxide, without interaction with the support, which vanishes after reduction above 300 ºC; (ii) two kinds of Ni^{2+} species in defective $Ni_{1-X}Al_2O_{4-X}$ (one in Ni-rich and the other in Al-rich environment) which contribution decreased upon reduction at above 600 ºC; and (iii) nickel in spinel phase, which can only be completely reduced at 850 ºC or above. Based on H_2-TPR data, Ni^{2+} species in Ni-rich mixed oxide phase (peak β_1), were more reducible [29]. Reduced Ni^{2+} species migrated to the solid surface leading to a framework enriched in Ni^{2+} species in Al-rich mixed oxide phase (β_2), as suggested by the decrease of the β_1/β_2 ratio (Table 2).

Under H_2 atmosphere, nickel diffused through the lattice of the non-stoichiometric spinel to form metallic Ni (Table 2). Ni diffusion continued until $Ni_{1-X}Al_2O_{4-X}$ was completely reduced, at around 700 ºC. Above that temperature, further Ni diffusion proceeded from stoichiometric $NiAl_2O_4$. A

similar behaviour was observed by Braidy et al. [34] with Ni doped alumina spinels prepared by wet-incipient method. They proposed that under reductive atmosphere, a continuous transition between $Ni_{1-X}Al_2O_{4-X}$ towards γ-alumina occurs as Ni leaves the matrix to form $NiAl_2O_4$ and eventually Ni. The intermediate formation of $NiAl_2O_4$ before metallic Ni, could explain the observed upturn in the contribution of $NiAl_2O_4$ in the NiAl-T series (Table 2). Previous research [24, 29], based on H_2-TPR analyses, concluded that Ni located in tetrahedral sites could be more difficult to reduce than Ni located in octahedral sites. Nevertheless, based on XRD, DRS-UV-vis and ^{27}Al-NMR data of our stoichiometric nickel aluminate spinels a different behaviour could be evidenced. That is, upon reduction, the number of tetrahedral nickel atoms diminished and increased that in octahedral sites). Regarding surface acid/basic properties, treatment under hydrogen flow caused surface enrichment in medium strength sites.

3.2. Catalytic performance experiments

Catalytic APR tests were performed at 250 ºC/45 bar in a bench-scale fixed-bed up-flow reactor. Bare γ-alumina and NiAl-c showed null activity (not shown). Blank tests with the reactor bed filled with quartz wool (employed to keep the bed fixed) showed no glycerol conversion, which suggested that homogeneous APR had no contribution to the catalytic conversion of glycerol. As a reference, the activity of bare Ni (obtained by reduction of NiO at 700 ºC for 1 h) was also evaluated.

Glycerol conversion (X_{Gly}) and carbon conversion to gas (X_{gas}) of NiAl-T catalysts in-situ reduced at temperature T are displayed in Figure 6A. Aqueous phase reforming of glycerol was negligible by reduced bare Ni catalysts which did not surpass conversion values of 3%. Raney Ni has been reported to be active for APR [45]. The very low performance of our bare nickel catalyst (in terms of X_{Gly} and X_{gas}) could be ascribed to its low surface area (less than 5 m^2/g).

Similarly, values for NiAl-350 and NiAl-450 remained below 5%. However, catalytic activity notably increased by increasing the catalysts' reduction temperature from 450 ºC to 600 ºC. For instance, glycerol conversion increased by a factor of 20 (NiAl-600: X_{Gly} = 66%). The most active assay was that reduced at 850 ºC with X_{Gly} = 93% (i.e. X_{Gly} increased by a factor of 1.4 with respect to NiAl-600). In addition, reduction at the highest temperature had a positive effect on the formation of gaseous products. The selectivity to gas (S_{gas}), that is, the percentage of carbon moles converted into gas phase per converted glycerol moles, was doubled in this temperature range: NiAl-600 (31%); NiAl-850 (62%), Figure 6A. Concomitantly, the exposed Ni metallic area increased by a factor of 5 (Table 2), NiAl-600/NiAl-450 = 0.48/0.10). Thus, the role of the available Ni^0 in the reforming activity seemed evident. At this point, it is interesting to note that the specific rate of hydrogen production, defined as the rate of hydrogen production per accessible nickel area, was maximum for

NiAl-600 (Figure 6B), which could be ascribed to its smallest metallic particle size (Table 1). It has been reported that partial oxidation of the surface of catalyst and the presence of metal oxide can facilitate dehydrogenation reactions [46]. Regarding particle size, both reforming and WGS reactions involve activation of water molecule. Alumina is able to activate water by forming hydroxyl groups. Nickel, in contrast to other metals such as Pt [47], is also capable of activating water via NiO formation [48]. Therefore, reactive Ni sites should be in close proximity to alumina, what would be more feasible over the smallest Ni particles.

FIGURE 6

TABLE 3

Data on Table 3 provide a comparison of the catalytic performance of our samples and others reported in the literature. In general terms, it is remarkable the high performance shown by our nickel aluminate catalysts when comparing with other nickel-based catalysts, in spite of the high space velocity (WHSV 24.5 h^{-1}) employed. The performance in terms of activity of our catalysts was even comparable to Pt-based catalysts, though, at lower selectivity to hydrogen, due to the inherent methanation activity of Ni. Indeed, it would be of interest to focus future research on increasing the selectivity to hydrogen (decrease selectivity to alkanes) of nickel aluminate-based catalytic system.

3.2.1. Gas phase products

The main products in the gas phase were hydrogen, carbon dioxide and methane, which accounted for more than 97% of the reaction products (in mol %), for all catalysts. Other minor compounds detected in the gas phase were alkanes (ethane, propane and C_{4+}) and carbon monoxide. Molar flow of gaseous products by catalysts NiAl-300 and NiAl-450 was very low, around 30 times lower than most active assays (Figure 7). The former catalysts produced a gas stream mainly composed by hydrogen (80-90% H_2). However, due to their low activity, because active sites are known to be the metallic nickel sites, hydrogen yield was very low (Y_{H2}= 0.7-1.4%, Table 4). For the catalysts reduced at 600 ºC or above, hydrogen yield notably increased (up to 21%) what, subsequently, favoured hydrogenolysis and hydrogenation reactions [56], as discussed in the liquid products section. Consequently, hydrogen concentration in the gas stream decreased, and levelled-off, at around 40-50% with a moderate formation of methane (i.e. 22%). It seems interesting to note that activity increased with reduction temperature in the 600 ºC to 850 ºC interval (i.e. amount of active sites increased, Table 2), however, the gas phase composition remained quite similar (Figure 7), what suggests that reaction mechanism did not vary substantially among the most active assays.

FIGURE 7

TABLE 4

The C-C scission ability of nickel was clearly evidenced from the large difference observed in the selectivity of C_1 (methane) and $C_2 + C_3$ alkanes (Table 4, Figure S5, Supporting Information), which implies that C-C scission activity was higher than dehydration/hydrogenation of the intermediate liquid compounds [57]. These results also suggested that a minimum amount of metallic Ni was required on catalyst surface to drive hydrogenolysis reactions. The metallic sites would ensure sufficient in-situ produced hydrogen for the hydrogenation of the liquid intermediate hydroxyacetone molecule. For instance, catalyst NiAl-450, with 0.1 m^2_{Ni}/g, mainly produced C_3 alkanes. This sample presented the highest acid to basic sites ratio (4.9, Table 1) which is beneficial for cleavage of C-O bonds [58]. However, catalyst NiAl-600 (~0.5 m^2_{Ni}/g) showed a selectivity of 17% to C_1 alkane (methane), with negligible formation of C_2 and C_3 alkanes. According to reaction network proposed (Scheme 1), methane was formed by CO hydrogenation, which requires metallic sites. The formation of methane was thermodynamically favoured, as CO hydrogenation reaction to methane is exothermic. As revealed by data in Table 4, H_2/CO_2 ratio remained below 7/3 (stoichiometric ratio in APR of glycerol) and decreased with reduction temperature. Indeed, this result supports that hydrogen was readily used in parallel reactions. Decarbonylation of intermediate liquid organic compounds formed CO molecules, which undergo WGS reaction to produce CO_2 and H_2 (Scheme 1). Indeed, Ni-based catalysts are reported to be active for the WGS reaction [59]. The low amount of CO obtained with our samples (Table 4) suggested that WGS was also favoured by $NiAl_2O_4$-derived catalysts to form H_2 and CO_2. C2 and higher alkanes could be formed through Fischer-Tropsch [8] and other reactions. For example, dehydration/hydrogenation of light alcohols can produce ethane and propane, while condensation reactions of intermediate liquid products can yield butane [60].

3.2.2. Liquid phase products

Molar flow of liquid products was negligible for catalysts NiAl-300 and NiAl-450, as well as for bare Ni, as due to their low catalytic activity. Catalyst reduced at 600 ºC produced around 0.7 $mmol_C/g_{cat}\cdot min$ of intermediate liquid products, which slightly decreased by increasing the reduction temperature (i.e. 0.53 $mmol_C/g_{cat}\cdot min$ for NiAl-850) (Figure 8A). This decline was ascribed to gasification of intermediate oxygenated hydrocarbon species by reforming reactions [8,61], as deduced from the concomitant increase in the conversion to gas.

FIGURE 8

SCHEME 1

The reaction network (Scheme 1) for the glycerol APR over bifunctional NiAl-T catalysts comprises two main routes: dehydrogenation to glyceraldehyde (route A), which requires metal sites, and dehydration to hydroxyacetone (route B), which requires acid sites. It is widely accepted that

hydroxyacetone is formed by elimination of primary hydroxyl group of glycerol, while 3-hydroxypropanal is formed by elimination of secondary hydroxyl group [62]. The fact that the later was no detected, was ascribed to the preponderant Lewis type acidity of our solids [62].

According to Figure 8A, the catalyst activation temperature strongly affected the selectivity to the liquid products. Catalysts reduced at low temperature (NiAl-300 and NiAl-450) mainly produced hydroxyacetone and very low amounts of small chain mono-alcohols (ethanol, methanol), suggesting that these catalysts favour dehydration reactions, as due to the scarcity of accessible nickel surface. The acid function was dominant in these catalysts (as revealed by a high ratio of acid/base sites). Consequently, hydroxyacetone was hardly hydrogenated to propylene glycol. In contrast, bare Ni, with only metallic function, produced a liquid stream mainly composed by methanol (73%) and an hydrogen-rich gaseous stream. According to Scheme 1, methanol was formed through decarbonylation reactions (route A), with CO (and H_2) release, which would be subsequently converted by WGS to yield more hydrogen and CO_2.

For catalysts reduced at 600 ºC or above, the main liquid products were glycols (1,2-propylene glycol and ethylene glycol), small chain mono-alcohols (ethanol and methanol), hydroxyacetone and, acetaldehyde in much lesser concentration. The observed liquid products distribution pointed to a complex process, where dehydrogenation, dehydration and hydrogenolysis reactions take place [6].

It should be noted that large amounts of glycols (sum of ethylene glycol and 1,2-propylene glycol) were produced, in the 47-59% range (Figure 8A), by all the active assays, indicative of C-O (i.e. 1,3-propylene glycol) and C-H and C-C (i.e. ethylene glycol) bond scission over Ni sites. Small amounts of 1-propanol and 2-propanol were also detected (less than 2%). These can be produced by additional dehydration and hydrogenation of 1,2-propylene glycol in the presence of hydrogen [63].

Liquid phase product distribution was notably affected by the catalyst activation temperature. Production of 1,2-propylene glycol and hydroxyacetone decreased as reduction temperature increased (1,2-propylene glycol: from 44% to 29%; hydroxyacetone: from 16% to 7%, both cases by NiAl-600 and NiAl-850, respectively). In contrast, the production of methanol and ethanol increased in similar intensity.

Figure 8B shows the evolution of the overall reaction products of route A with respect to all reaction products of route B. That is, the sum of total products of dehydrogenation (methanol, ethylene glycol and ethanol) and dehydration (hydroxyacetone and 1,2-propylene glycol) reactions are depicted. A clear trend could be observed where an increase in the reduction temperature enhanced the production of dehydrogenation products. In contrast, a concomitant decrease of dehydration/hydrogenation products could be confirmed. For instance, for catalysts reduced at below 600 ºC

dehydration/hydrogenation products accounted for 39% of APR products, which increased up to 61% at the highest reduction temperature. From Figure 8B it could be concluded that at above 700 ºC, route A prevailed. This confirms the relevant role of metallic sites in determining the dominant route in the APR of glycerol. The fact that route A (dehydrogenation-decarbonylation) was the main mechanism reflected that C-H and C-C scission by hydrogenolysis was favoured, in detriment of C-O cleavage, as also reported by others [64]. Gandarias et al. [65] studied the effect of the incorporation of Cu into Ni/Al_2O_3 catalysts. They concluded that the reduction in size of the Ni ensembles inhibited the C-C bond cleavage. This effect should not be discarded for our catalytic system.

The formation of Ni-C bond requires a previous dehydrogenation of glycerol in order to be adsorbed on Ni metal [64]. The high selectivity to hydroxyacetone suggested that this mechanism prevailed for catalyst NiAl-300 and NiAl-450, probably due to its low hydrogen yield. If hydrogen partial pressure increases (i.e. due to in-situ formation), both hydrogen and glycerol can adsorb on Ni sites. Then, after protonation of hydroxyl group by metallic acidic sites [66], the cleavage of C-O bond would proceed followed by hydrogen transfer from Ni to the carbon, resulting in 1,2-propylene glycol formation, which was observed for catalysts reduced at 600 ºC or above. The occurrence of this route would be supported by the presence of propanols, which were formed through the dehydration/hydrogenation of 1,2-propylene glycol (Scheme 1). However, the small amounts of propanols and acetone (less than 0.8 mol%) reflected the 1,2-propylene glycol was the final liquid product by this route, since further decomposition would require acid sites for dehydration to acetone or propionaldehyde. Experimental data pointed to the preponderance of metallic function with respect to acid function in the investigated catalytic system.

Ethanol can be formed through hydrogenation of the acetaldehyde molecule [67] (Scheme 1). The low amount of acetaldehyde produced by our active catalysts revealed the feasibility of this route. By increasing reduction temperature, H_2/CO_2 ratio slightly decreased, as shown in Table 4, as the yield to ethanol increased. This result suggested that for catalysts reduced at the highest temperatures (700 and 850 ºC) hydrogen yield increased, however, a larger fraction of the in-situ formed hydrogen was consumed in hydrogenolysis reactions. Catalyst NiAl-850 showed to be the best catalyst in terms of glycerol conversion and hydrogen yield for the aqueous phase reforming of 10 wt.% glycerol. However, it seems interesting to note that the intrinsic activity of the Ni active sites was largest for NiAl-600 (Figure 6B). It could be concluded that catalyst reduced at the highest temperature consumed more hydrogen in parallel reactions with superior methane formation. It would be of interest to gain knowledge on the properties required to improve the intrinsic activity of the catalyst reduced at the highest temperature. It is likely that adequate surface acid/base properties of the nickel

aluminate catalyst could allow tuning the selectivity towards dehydrogenation reactions rather than hydrogenolysis.

3.2.3. Effect of working Temperature/Pressure conditions

Catalytic tests were performed at 235 ºC/35 bar, 250 ºC/45 bar and 260 ºC/52 bar over in-situ reduced NiAl-T catalysts. As shown in Figure 9A (and Table S3, Supporting Information), independent of the operation conditions, activity was negligible for catalysts NiAl-350 and NiAl-450, which did not surpass conversion values of 5%. The performance of the rest of catalysts, in terms of conversion of glycerol and gasification activity, improved at the most severe APR conditions, in agreement with literature [13,46]. For example, X_{gas} increased by 31% (NiAl-450), 63% (NiAl-600), 74% (NiAl-700) and 79% (NiAl-850) by changing from 235 ºC/35 bar to 260 ºC/52 bar. Concomitantly, S_{gas} increased by 22% (NiAl-600), 30% (NiAl-700) and 38% (NiAl-850). Hydrogen yield also increased (Table S3, Supporting Information), due to enhanced C-C and C-O bond cleavage promoted by temperature increase [68,69].

Apparent activation energy was estimated assuming first order reaction kinetics. The obtained values (Figure 9A)**,** ranged between 75-110 kJ/mol, reflecting the weight of catalyst configuration on reaction mechanism. The increasing trend in the Ea suggests that the reactions over metallic nickel sites were characterized by a higher activation energy than those occurring over the acid sites.

FIGURE 9

The concentration of H_2 and CH_4 in the gas stream (Table S3, Supporting Information) slightly varied with T/P conditions, and a trade-off could be deduced between both species. This way, as T/P varied from 235 ºC/35 bar to 260 ºC/52 bar, the H_2 concentration in the gas stream vaguely decreased: 54% to 52% (NiAl-600); 53% to 45% (NiAl-700); 48% to 43% (NiAl-850), while CH_4 concentration increased as: 20% to 21% (NiAl-600); 19% to 24% (NiAl-700); 20% to 25% (NiAl-850). Accordingly, H_2/CO_2 ratio declined (Table S3, Supporting Information) what reflected hydrogen consumption in parallel reactions, such as CO methanation, as revealed by increased selectivity to methane.

The alkane selectivity as a function of C number followed similar distribution with reaction T/P, the highest selectivity being for C1 alkanes (methane) for the three T/P operation conditions (Figure S5, Supporting Information). At most severe conditions selectivity to methane increased, especially at the highest reduction temperature.

Liquid phase composition of active catalysts also varied with the reaction T/P conditions (Figure 9B), while for catalyst NiAl-450 it was almost unaffected. Moreover, the effect of T/P became more intense as reduction temperature increased (i.e. the activation energy). A trade-off between small

563 chain alcohols (which increased) and glycols (which decreased) was observed with the increase of
564 T/P, with almost constant formation of hydroxyacetone.

565 The ratio between overall reaction products of route A with respect to route B was above 1 for
566 NiAl-700 and NiAl-850 catalysts, and below 1 for the rest of catalysts. In addition, it increased with
567 reaction T/P conditions, except for NiAl-450 (Figure S6, Supporting Information). For example,
568 changing from 235 ºC/35 bar to 260 ºC/52 bar, it increased from 1.1 to 2.9 for NiAl-850 catalyst, and
569 at lesser extent for NiAl-600 (from 0.5 to 0.7). This behaviour could be interpreted as that most severe
570 conditions favoured decarbonylation and C-C scission over C-O scission [70].

571 3.2.4. Long-term experiments

572 Catalytic performance (i.e. glycerol conversion, conversion to gas and selectivity to gas) as a function
573 of time-on-stream (TOS) was investigated for catalysts NiAl-700 and NiAl-850, under mild
574 conditions (235 ºC/35 bar) for a period of 50 h. As shown in Figure 10 both catalysts followed a
575 similar trend, with a sustained loss of activity over the whole catalytic test, being more pronounced
576 during the first hours of operation (i.e. 8 h TOS). An overall decay of around 45% and 60% was
577 observed in the glycerol conversion and conversion to gas, respectively. S_{gas} also decreased with TOS,
578 and after 20 h, it levelled-off at around 61% and 73% for NiAl-700 and NiAl-850, respectively. The
579 stability of these catalysts can be deemed as good as compared to other nickel supported catalysts.
580 For example, Shabaker et al. [45] reported 90% of initial activity decay during 48 hours of APR of
581 ethylene glycol over Ni supported on different supports, among them γ-alumina, and attributed to
582 metal sintering. Thus, catalysts prepared by activation of spinel-based precursors showed promising
583 stability results, as compared to traditional impregnation methods.

584 FIGURE 10

585 Figure 11 depicts the evolution with TOS of several reaction parameters related to the selectivity of
586 the APR reaction of NiAl-700 and NiAl-850 catalysts. Selectivity to hydrogen increased, particularly
587 after 20-30 h of TOS. The yield to hydrogen, however, remained stable due to the counter effect of
588 the loss of activity. Concomitantly, selectivity to methane decreased as reaction proceed, particularly
589 for NiAl-700 (Figures 11A and B).

590 The total molar flow of gaseous products dropped-off by around 26% for both catalysts after 50 h of
591 operation. The gas stream enriched in hydrogen with TOS, and both H_2/CO_2 and H_2/CH_4 ratios
592 increased (Figures 11A and B). The opposite trend was observed on H_2/CO, especially for catalyst
593 NiAl-700. H_2/CO decreased by around 36% for catalyst NiAl-850 and up to 65% for NiAl-700. This
594 is consistent with a limited occurrence of WGS as TOS increased. It is known the high CO and CO_2
595 hydrogenation [71] and WGS [47] activity of metallic Ni. In both reactions, the C-containing

molecule is firstly activated onto the metallic site [72]. The observed data suggested that the severe hydrothermal conditions of APR inhibit the CO activation capacity of Ni. The fact that NiAl-700 contained half the amount of Ni^0 of NiAl-850 would make it more sensitive to deactivation.

FIGURE 11

Regarding intermediate liquid products, both NiAl-700 and NiAl-850 showed similar trend, where hydroxyacetone formation increased and ethylene glycol, ethanol and methanol decreased with TOS (Figure 11C). This behaviour revealed a decreasing trend in the (Scheme 1) route A/route B product distribution, which varied from 1.1 to 0.7 for NiAl-700 and from 0.85 to 0.6 for NiAl-850, indicative of a loss of metal function.

3.3. Characterization of spent catalysts

The spent catalysts were analysed in order to elucidate the main factors that contribute to catalyst deactivation. The nickel re-oxidation and lixiviation, the structural changes in the catalysts and the formation of carbonaceous deposits were analysed.

The specific surface area of the spent catalysts increased (Table 1), more markedly for samples reduced at higher temperature. The used samples showed bimodal pore size distribution (Figure S1B, Supporting Information), which would be related to the coexistence of both boehmite and nickel aluminate phases.

H_2-TPR analysis of spent NiAl-T catalysts (named as NiAl-T-u) are shown in Figure 1B, and the obtained values are given in Table S4, Supporting Information. Catalysts NiAl-300-u showed an incipient peak below 500 ºC, indicative of nickel re-oxidation. Samples reduced at $T \geq 600$ ºC showed a substantial low-temperature hydrogen consumption what reflected that re-oxidation of metallic Ni took place to a greater extent. Reduction at 250 ºC suggested coalescence into large NiO particles as due to high free surface energy. The less intense, unresolved peaks in the 300-600 ºC range observed for samples NiAl-700 and NiAl-850 were ascribed to the reduction of smaller NiO particles interacting with the support or to nickel defective spinel compounds. The subtle reduction peak of catalyst NiAl-850 at about 750 ºC suggested that part of the Ni was re-oxidized to the original spinel structure, facilitated by the open spinel structure of γ-alumina that hosted the Ni^{2+} species [73]. TPR analyses quantified this amount at around 4.2% of the loaded Ni. Note that the high temperature hydrogen consumption (at around 775 ºC) of NiAl-700 indicated the existence of nickel aluminate spinel, yet unreduced in the fresh catalyst. For these most active catalysts, overall, around 45% of the metallic Ni in fresh catalyst was re-oxidised (Table 2). Yet, we have no clear evidence to explain the larger than 100% re-oxidation measured for catalyst NiAl-600. We hypothesize it could be caused by leaching of Ni atoms located in the spinel structure, and subsequent re-deposition on the surface [37].

[74] employed Ni/alumina prepared by wetness impregnation for the ethylene glycol reforming, and also acknowledged the nickel oxidation as the main cause of deactivation.

The reduction profiles of catalysts used for 50 h (NiAl-700-50h and NiAl-850-50h, Figure 1B) were qualitatively very similar to those used for 2 h. In the spent catalyst, around 34% of the initial Ni was re-oxidized, what indicated that most of the metallic Ni in our catalytic system was oxidized during initial stages of APR. This would explain the previously noted initial fast activity decay (Figure 10). Thereafter, these species were progressively leached out, and around 7% of the metal loaded was lost during the long-term catalytic run (Table 1).

XRD analysis of the used samples revealed the presence of boehmite phase (Figure 2B, Table 1) in spent catalysts. The characteristic peaks intensity increased with reduction temperature, probably due to increasing content of γ-Al_2O_3 in fresh catalysts and its transformation into boehmite. Indeed, the acidity of the reaction medium increased with time (feed pH: 8; collected liquid product after 2 h TOS pH: 4, as due to the dissolved CO_2), enhancing the hydration of γ-alumina. Formation of boehmite was also confirmed by FTIR of the spent catalysts (Figure S3B, Supporting Information). For the samples reduced at 700 and 850 ºC, NiO was also detected by XRD, which confirmed the re-oxidation of nickel surface, in agreement with TPR results.

The amount of exposed Ni area dramatically dropped after APR tests (Table 2). For example, the exposed Ni area for the most active catalyst NiAl-850 decreased from 3.47 m^2/g (fresh catalyst) to 0.23 m^2/g (2 TOS), what represents a 93% decrease. However, the observed leaching and particle migration and sinterization cannot explain such a drop in the exposed area. This observation could be the result of the formation of core-shell particles under APR conditions [75], comprised of metallic Ni core and metal oxide shell. The catalytic activity decay was in line with the amount of re-oxidized Ni as measured from TPR analysis.

Regarding the nickel particle growth, it occurred rapidly, as determined by XRD analysis. For example, after two hours of TOS, particle size increased from around 8-14 nm to 42-46 nm (Table 1). Thereafter, it did not substantially increase after 50 h of usage (for example, for NiAl-850 catalyst, metallic nickel crystallite size was 44.1 nm). The opposite trend observed for NiAl-700 catalyst suggests leaching of larger particles, what is in direct contradiction with that reported by others where small particles are main source of leached species [74]. Nickel particles of NiAl-600 with the initial smaller particle size outgrow those of samples NiAl-700 and NiAl-850, and all the spent catalysts ended up with similar particle size. This is consistent with theories on particle migration [74] where the initial particle growth rate is larger for smaller particles, and the rates decrease as the average particle size increases. It appeared that the average Ni particle size of spent catalysts was not significantly affected by the activation temperature. However, a subtle decreasing trend could be

663 deduced as reduction temperature increased, what could be ascribed to stronger interaction of Ni
664 particles with the support.

665 Leaching of Ni and Al was also considered given the acidity of the reaction medium (pH decreased
666 to 4 with TOS). The ICP data (Table 1) revealed that leaching of Al from the support was negligible.
667 Leaching of Ni occurred during APR, however, it was minimal even under high glycerol conversion
668 conditions (i.e. about 0.2% Ni leached for NiAl-850 catalyst).

669 Spent catalyst after 50 h TOS contained small amounts of carbonaceous deposits (0.2-1.0 $mmol_C/g$)
670 (Table 1), lesser than typical values reported in the literature (up to 10 $mmol_C/g$) [61,76], which makes
671 the nickel aluminate spinel-derived catalysts resistant to deactivation by coke. Morever, XRD of spent
672 catalysts (Figure 2B) showed the absence of diffraction peaks of graphitic carbon, reflecting its low
673 content.

674 Based on the characterisation of spent catalysts, it seemed that the main causes of activity decay were
675 nickel re-oxidation and sintering, while metal leaching and coke formation had subtle effect.

676 **3. Conclusions**

677 Stoichiometric bulk nickel aluminate spinel was prepared by coprecipitation and calcination at
678 850 ºC. The effect of reduction temperature, between 300 and 850 ºC, on physichochemical properties
679 and catalytic performance in the APR of glycerol were investigated.

680 Results clarify that pore volume was hardly affected upon reduction (300-850 ºC), with minor
681 alterations in specific area and average pore size. Also, XRD, DRS-UV and FTIR analyses confirmed
682 the good stability of the spinel structure. The used coprecipitation method led to defective Ni-Al
683 mixed oxides, where metallic nickel diffused to the solid surface, strongly interacting with the bulk,
684 what provided very small metallic nickel particles (< 14 nm). It was noticed that hydrogen treatment
685 increased surface density of medium strength acid and basic sites, in detriment of weak and strong
686 sites.

687 It is remarkable the high performance shown by our nickel aluminate catalysts in glycerol APR, in
688 spite of the high space velocity (WHSV 24.5 h^{-1}). The most active assay was that reduced at 850 ºC
689 with 93% glycerol conversion, 57% conversion to gas and 62% selectivity to gas (at 250 ºC/45 bar).
690 The maximum specific hydrogen production rate was achieved upon reduction at 600 ºC, due to
691 adequate ratio between Ni^0 and accessible support.

692 For all the prepared assays, hydrogen was the main compound in the gaseous stream, followed by
693 carbon dioxide and methane. The low formation of CO suggested that WGS was also favoured by

694 our $NiAl_2O_4$-derived catalysts to form H_2 and CO_2. Other small chain alkanes were hardly detected
695 what evidenced the high C-C scission ability of the investigated catalysts.

696 Reduction temperature had a more marked effect on the liquid phase product distribution. Results
697 suggested a key contribution of accessible metallic sites and medium strength acidic sites to the
698 overall reaction scheme, with the glycerol reforming occurring through both the dehydrogenation to
699 glyceraldehyde, and through dehydration of terminal hydroxyl groups, and subsequent hydrogenation
700 to yield 1,2-propylene glycol. Activation at 700 ºC or above favoured dehydrogenation mechanism,
701 whereas dehydration/hydrogenation mechanism was dominant for catalysts reduced below 600 ºC.

702 Long term catalytic runs revealed the good durability of Ni aluminate spinel catalysts, where
703 deactivation occurred mainly though nickel re-oxidation and sinterization, which, indeed, modified
704 the distribution of gas and intermediate liquid products with TOS.

705 **Acknowledgements**

706 This work is supported by ENE2016-74850-R Mineco and Feder project. A.M.M. thanks Mineco for
707 her pre-doctoral grant (BES-2014-069965). Likewise, the authors thank for the technical support
708 provided by SGIker of UPV/EHU and European funding (ERDF and ESF)

709 **4. References**

710 [1] L.C. Meher, D. Vidya Sagar, S.N. Naik, Technical aspects of biodiesel production by
711 transesterification-a review, Renew. Sust. Energ. Rev. 10(3) (2006) 248-268

712 [2] G.T. Jeong, H.S. Yang, D.H. Park, Optimization of transesterification of animal fat ester using
713 response surface methodology, Bioresour. Technol. 100(1) (2009) 25-30

714 [3] M.I. Al-Widyan, A.O. Al-Shyoukh, Experimental evaluation of the transesterification of waste
715 palm oil into biodiesel, Bioresour. Technol. 85(3) (2002) 253-256

716 [4] R. Ciriminna, C. Della Pina, M. Rossi, M. Pagliaro, Understanding the glycerol market, Eur. J.
717 Lipid Sci. Technol. 116 (2014) 1432–1439

718 [5] C.H. Zhou, J.N. Beltramini, Y.X. Fan, G.Q. Lu, Chemoselective catalytic conversion of glycerol
719 as a biorenewable source to valuable commodity chemicals, Chem. Soc. Rev. 37 (2008) 527-549

720 [6] N.H. Tran, G.S. Kannangara, Conversion of glycerol to hydrogen rich gas, Chem. Soc. Rev.
721 42(24) (2013) 9454-9479

722 [7] R.D. Cortright, R.R. Davda, J.A. Dumesic, Hydrogen from catalytic reforming of biomass-derived
723 hydrocarbons in liquid water, Nature 418 (2002) 964–967

724 [8] R.R. Davda, J.W. Shabaker, G.W. Huber, R.D. Cortright, J.A. Dumesic, A review of catalytic
725 issues and process conditions for renewable hydrogen and alkanes by aqueous-phase reforming of
726 oxygenated hydrocarbons over supported metal catalysts, Appl. Catal. B:Environ. 56 (2005) 171-186

[9] M. El Doukkali, A.Iriondo, P.L. Arias, J. Requies, I. Gandarías, L. Jalowiecki-Duhamel, F. Dumeignil, A comparison of sol–gel and impregnated Pt or/and Ni based γ-alumina catalysts for bioglycerol aqueous phase reforming, Appl. Catal. B:Environ. 125 (2012) 516-529

[10] Y.C. Lin, Review: Catalytic valorization of glycerol to hydrogen and syngas, Int. J. Hydrogen Energ. 38(6) (2013) 2678-2700

[11] R.L. Manfro, A.F. da Costa, N.F.P. Ribeiro, M.M.V.M. Souza, Hydrogen production by aqueous-phase reforming of glycerol over nickel catalysts supported on CeO_2, Fuel Process. Technol. 92(3) (2011) 330-335

[12] G. Wen, Y. Xu, H. Ma, Z. Xu, Z. Tian, Production of hydrogen by aqueous-phase reforming of glycerol, Int. J. Hydrogen Energ. 33(22) (2008) 6657-6666

[13] R.L. Manfro, T.P.M.D. Pires, N.F.P. Ribeiro, M.M.V.M. Souza, Aqueous-phase reforming of glycerol using Ni–Cu catalysts prepared from hydrotalcite-like precursors, Catal. Sci. Technol. 3 (2013) 1278-1287

[14] A. Iriondo, V.L. Barrio, J.F. Cambra, P.L. Arias, M.B. Güemez, R.M. Navarro, M.C. Sánchez-Sánchez, J.L.G. Fierro, Hydrogen Production from Glycerol Over Nickel Catalysts Supported on Al_2O_3 Modified by Mg, Zr, Ce or La, Top. Catal. 49(1) (2008) 46-58

[15] J. Remón, J.R. Giménez, A. Valiente, L. García, J. Arauzo, Production of gaseous and liquid chemicals by aqueous phase reforming of crude glycerol: Influence of operating conditions on the process, Energy Convers. Manag. 110 (2016) 90-112

[16] A. Seretis, P.Tsiakaras, Crude bio-glycerol aqueous phase reforming and hydrogenolysis over commercial SiO_2-Al_2O_3 nickel catalyst, Renew. Energ. 97 (2016) 373-379

[17] Y. Kathiraser, W. Thitsartarn, K. Sutthiumporn, S. Kawi, Inverse $NiAl_2O_4$ on $LaAlO_3$–Al_2O_3: Unique Catalytic Structure for Stable CO_2 Reforming of Methane, J. Phys. Chem. C 117(16) (2013) 8120–8130

[18] R.M. Ravenelle, J.R. Copeland, W.G Kim, John C. Crittenden, C. Sievers, Structural Changes of γ-Al_2O_3-Supported Catalysts in Hot Liquid Water, ACS Catal. 1(5) (2011) 552–561

[19] C. Jiménez-González, Z. Boukha, B. de Rivas, J.J. Delgado, M.A. Cauqui, J.R. González-Velasco, J.I. Gutiérrez-Ortiz, R. López-Fonseca, Structural characterisation of Ni/alumina reforming catalysts activated at high temperatures, Appl. Catal. A:Gen. 466 (2013) 9–20

[20] H. Özdemir, M.A.F. Öksüzömer, M.A. Gürkaynak, Effect of the calcination temperature on Ni/$MgAl_2O_4$ catalyst structure and catalytic properties for partial oxidation of methane, Fuel 116 (2014) 63-70

[21] H.S.C. O'Neill, W. A. Dollase, C. R. Ross II, Temperature dependence of the cation distribution in nickel aluminate ($NiAl_2O_4$) spinel: a powder XRD study, Phys. Chem. Minerals 18 (1991) 302-319

[22] A. Khan, P.G. Smirniotis, Relationship between temperature-programmed reduction profile and activity of modified ferrite-based catalysts for WGS reaction, J. Mol. Catal. A:Chem. 280(1–2) (2008) 43-51

[23] F.P. Ribeiro, R.C.R. Neto, S.F. Moya, M.M.V.M. Souza, M. Schmal, Synthesis of $NiAl_2O_4$ with high surface area as precursor of Ni nanoparticles for hydrogen production, Int. J. Hydrogen Energ. 35(21) (2010) 11725-11732

[24] Z. Boukha, C. Jiménez-González, B. de Rivas, J.R. González-Velasco, J.I. Gutiérrez-Ortiz, R. López-Fonseca, Synthesis, characterisation and performance evaluation of spinel-derived Ni/Al_2O_3 catalysts for various methane reforming reactions, Appl. Catal. B:Environ. 158–159 (2014) 190–201

[25] M.C.J. Bradford, M.A. Vannice, Catalytic reforming of methane with carbon dioxide over nickel catalysts II. Reaction kinetics, Appl. Catal. A:Gen. 142 (1996) 97–122

[26] J.S. Smith, P.A. Thrower, M.A. Vannice, Characterization of $NiTiO_2$ catalysts by TEM, X-ray diffraction, and chemisorption techniques, J. Catal. 68 (1981) 270–285

[27] J.C. Ganley, F.S. Thomas, E.G. Seebauer, R.I. Masel, A Priori Catalytic Activity Correlations: The Difficult Case of Hydrogen Production from Ammonia, Catal. Lett. 96 (2004) 117

[28] C.H. Bartholomew, Mechanisms of catalyst deactivation, Appl. Catal. A:Gen. 212(1–2) (2001) 17-60

[29] G. Li, L. Hu, J.M. Hill, Comparison of reducibility and stability of alumina-supported Ni catalysts prepared by impregnation and co-precipitation, Appl. Catal. A:Gen. 301(1) (2006) 16-24

[30] J.L. Rogers, M.C. Mangarella, A.D. D'Amico, J.R. Gallagher, M.R. Dutzer, E. Stavitski, J.T. Miller, C. Sievers, Differences in the Nature of Active Sites for Methane Dry Reforming and Methane Steam Reforming over Nickel Aluminate Catalysts, ACS Catal. 6(9) (2016) 5873–5886

[31] A. Tirsoaga, D. Visinescu, B. Jurca, A. Ianculescu, O. Carp, Eco-friendly combustion-based synthesis of metal aluminates MAl_2O_4 (M 5 Ni, Co), J. Nanopart. Res. 13 (2011) 6397–6408

[32] L. Zhou, L. Li, N. Wei, J. Li, J.M. Basset, Effect of $NiAl_2O_4$ Formation on Ni/Al_2O_3 Stability during Dry Reforming of Methane, ChemCatChem 7(16) (2015) 2508-2516

[33] Z. Skoufa, G. Xantri, E. Heracleous, A.A. Lemonidou, A study of Ni–Al–O mixed oxides as catalysts for the oxidative conversion of ethane to ethylene, Appl. Catal. A:Gen. 471 (2014) 107-117

[34] N. Braidy, S. Bastien, J. Blanchard, C. Fauteux-Lefebvre, I. E. Achouri, N. Abatzoglou, Activation mechanism and microstructural evolution of a YSZ/Ni-alumina catalyst for dry reforming of methane, Catal. Today 291 (2017) 99-105

[35] J. Zhang, H. Xu, X. Jin, Q. Ge, W. Li, Characterizations and activities of the nano-sized Ni/Al_2O_3 and $Ni/La–Al_2O_3$ catalysts for NH_3 decomposition, Appl. Catal A: Gen 290(1–2) (2005) 87-96

[36] Y.S. Han, J.B. Li, X.S. Ning, B. Chi, Effect of Preparation Temperature on the Lattice Parameter of Nickel Aluminate Spinel, J. Am. Ceram. Soc. 87(7) (2004) 1347–1349

[37] G. Wen, Y, Xu, Z. Xu, Z. Tian, Characterization and Catalytic Properties of the Ni/Al_2O_3 Catalysts for Aqueous-phase Reforming of Glucose, Catal. Lett. 129 (2009) 250–257

[38] E. Heracleous, A.F. Lee, K. Wilson, A.A. Lemonidou, Investigation of Ni-based alumina-supported catalysts for the oxidative dehydrogenation of ethane to ethylene: structural characterization and reactivity studies, J. Catal. 231(1) (2005) 159-171

[39] J. Wang, L. Dong, Y. Hu, G. Zheng, Z. Hu, Y. Chen, Dispersion of NiO Supported on γ-Al_2O_3 and TiO_2/γ-Al_2O_3 Supports, J. Solid State Chem. 157(2) (2001) 274–282

[40] J. L. Cuya Huaman, N. Hironaka, S. Tanaka, K. Shinoda, H. Miyamura, B. Jeyadevan, Size-controlled monodispersed nickel nanocrystals using 2-octanol as reducing agent, CrystEngComm 15 (2013) 729-737

[41] A. Tribalis, G. D. Panagiotou, K. Bourikas, L. Sygellou, S. Kennou, S. Ladas, A. Lycourghiotis, C. Kordulis, Ni Catalysts Supported on Modified Alumina for Diesel Steam Reforming, Catalysts 6(1) (2016) 11-24

[42] H. Deng, Y.Yu, H. He, The role of AgOAl entities in adsorption of NCO species and reduction of NOx, Catal. Today 258(1) (2015) 35-40

[43] R. Estevez, S. Lopez-Pedrajas, F. Blanco-Bonilla, D. Luna, F. M. Bautista, Production of acrolein from glycerol in liquid phase on heterogeneous catalysts, Chem. Eng. J. 282 (2015) 179–186

[44] B.C. Miranda, R.J. Chimentão, F. Gispert-Guirado, J. Llorca, F. Medina, F. LópezBonillo, J.E. Sueiras, Conversion of glycerol over 10%Ni/γ-Al_2O_3 catalyst, Appl. Catal. B:Environ. 147 (2014) 464-480

[45] J.W. Shabaker, G.W. Huber, J.A. Dumesic, Aqueous-phase reforming of oxygenated hydrocarbons over Sn-modified Ni catalysts, J. Catal. 222(1) (2004) 180-191

[46] E.B. Pereira, N. Homs, S. Martí, J.L.G. Fierro, P. Ramírez de la Piscina, Oxidative steam-reforming of ethanol over Co/SiO_2, $Co\text{-}Rh/SiO_2$ and $Co\text{-}Ru/SiO_2$ catalysts: Catalytic behavior and deactivation/regeneration processes, J. Catal., 257(1) (2008) 206-214

[47] D.C. Grenoble, M.M. Estadt, D.F. Ollis, The chemistry and catalysis of the water gas shift reaction: 1. The kinetics over supported metal catalysts, J. Catal. 67(1) (1981) 90-102

[48] J.R. Rostrup-Nielsen, Catalytic Steam Reforming, Springer-Verlag, Berlin, 1984

[49] F. Bastan, M. Kazemeini, A. Larimi, H. Maleki, Production of renewable hydrogen through aqueous-phase reforming of glycerol over Ni/Al_2O_3MgO nano-catalyst, Int. J. Hydrogen Energ. 43(2) (2018) 614-62

[50] Y.H. Park, J.Y. Kim, D.J. Moon, N.C. Park, Y.C. Kim, Effect of $LaAlO_3$-supported modified Ni-based catalysts on aqueous phase reforming of glycerol, Res. Chem. Intermediat., 41(12) (2015) 9603-9614

[51] M.M. Rahman, T.L. Church, M.F. Variava, A.T. Harris, A.I. Minett, Bimetallic Pt–Ni composites on ceria-doped alumina supports as catalysts in the aqueous-phase reforming of glycerol, RSC Adv., 4 (2014) 18951-18960

[52] F. Bastan, M. Kazemeini, A.S. Larimi, Aqueous-phase reforming of glycerol for production of alkanes over $Ni/Ce_xZr_{1-x}O_2$ nano-catalyst: Effects of the support's composition, Renew. Energ. 108 (2017) 417-424

[53] D.L. King, L. Zhang, G. Xia, A.M. Karim, D.J. Heldebrant, X. Wang, T. Peterson, Y. Wang, Aqueous phase reforming of glycerol for hydrogen production over Pt–Re supported on carbon, Appl. Catal B: Environ. 99(1-2) (2010) 206-213

[54] C. Pendem, B. Sarkar, N. Siddiqui, L.N.S. Konathala, C. Baskar, R. Bal, K-Promoted Pt-Hydrotalcite Catalyst for Production of H_2 by Aqueous Phase Reforming of Glycerol, ACS Sustainable Chem. Eng. 6(2) (2018) 2122-2131

[55] Y. Guo, M.U. Azmat, X. Liu, Y. Wang, G. Lu, Effect of support's basic properties on hydrogen production in aqueous-phase reforming of glycerol and correlation between WGS and APR, Appl. Energ., 92 (2012) 218-223

[56] S. Liu, M. Tamura, Z. Shen, Y. Zhang, Y. Nakagawa, K. Tomishige, Hydrogenolysis of glycerol with in-situ produced H_2 by aqueous-phase reforming of glycerol using Pt-modified Ir-ReOx/SiO_2 catalyst, Catal. Today 303 (2018) 106-116

[57] G.W. Huber, R.D. Cortright, J.A. Dumesic, Renewable Alkanes by Aqueous-Phase Reforming of Biomass-Derived Oxygenates, Angew. Chem. Int. Ed. 43(12) (2004) 1549-1551

[58] A. Ciftci, S. Eren, D.A.J.M. Ligthart, E.J.M. Hensen, Platinum-Rhenium Synergy on Reducible Oxide Supports in Aqueous Phase Glycerol Reforming, ChemCatChem 6 (2014) 1260-1269

[59] L. Bobrova, D. Andreev, E. Ivanov, N. Mezentseva, M. Simonov, L. Makarshin, A. Gribovskii, V. Sadykov, Water-Gas Shift Reaction over Ni/CeO_2 Catalysts, Catalysts 7(10) (2017) 310-334

[60] L.I. Godina, A.V. Tokarev, I.L. Simakova, P. Mäki-Arvela, E. Kortesmäki, J. Gläsel, L. Kronberg, B. Etzold, D.Y. Murzin, Aqueous-phase reforming of alcohols with three carbon atoms on carbon-supported Pt, Catal. Today 301 (2018) 78-89

[61] N. Luo. X. Fu, F. Cao, T. Xiao, P.P. Edwards, Glycerol aqueous phase reforming for hydrogen generation over Pt catalyst – Effect of catalyst composition and reaction conditions, Fuel 87(17–18) (2008) 3483-3489

[62] A. Talebian-Kiakalaieh, N.A.S. Amin, H. Hezaveh, Glycerol for renewable acrolein production by catalytic dehydration, Renew. Sust. Energ. Rev. 40 (2014) 28-59

[63] I. Gandarias, P.L. Arias, J. Requies, M.B. Güemez, J.L.G. Fierro, Hydrogenolysis of glycerol to propanediols over a Pt/ASA catalyst: The role of acid and metal sites on product selectivity and the reaction mechanism, Appl. Catal. B:Environ. 97 (1-2) (2010) 248-256

[64] Y.S. Yun, D.S. Park, J. Yi, Effect of nickel on catalytic behaviour of bimetallic Cu-Ni catalyst supported on mesoporous alumina for the hydrogenolysis of glycerol to 1,2-propanediol, Catal. Sci. Technol. 4 (2014) 3191-3202

[65] I. Gandarias, J. Requies, P.L. Arias, U. Armbruster, A. Martin, Liquid-phase glycerol hydrogenolysis by formic acid over Ni-Cu/Al_2O_3 catalysts, J. Catal. 290 (2012) 79-89

[66] I. Gandarias, P.L. Arias, J. Requies, M. El Doukkali, M.B. Güemez, Liquid-phase glycerol hydrogenolysis to 1,2-propanediol under nitrogen pressure using 2-propanol as hydrogen source, J. Catal. 282(1) (2011) 237-247

[67] A.K. Agarwal, M.S. Wainwright, D.L. Trimm, N.W. Cant, Acetaldehyde hydrogenation over a Cu/SiO_2 catalyst, J. Mol. Catal. 45(2) (1988) 247-254

[68] A.V. Kirilin, A.V. Tokarev, E.V. Murzin, L.M. Kustov, J.P. Mikkola, D.Y. Murzin, Reaction Products and Transformations of Intermediates in the Aqueous Phase Reforming of Sorbitol, ChemSusChem 3(6) (2010) 708-718

[69] A. Seretis, P. Tsiakaras, Aqueous phase reforming (APR) of glycerol over platinum supported on Al_2O_3 catalyst, Renew. Energy 85 (2016) 1116-1126

[70] M.A. Dasari, P.P. Kiatsimkul, W.R. Sutterlin, G.J. Suppes, Low-pressure hydrogenolysis of glycerol to propylene glycol, Appl. Catal. A:Gen. 281(1–2) (2005) 225-231

[71] V. Shadravan, E. Kennedy, M. Stockenhuber, An experimental investigation on the effects of adding a transition metal to Ni/Al_2O_3 for catalytic hydrogenation of CO and CO_2 in presence of light alkanes and alkenes, Catal. Today 307 (2018) 277-285

[72] J. Sehested, S. Dahl, J. Jacobsen, J.R. Rostrup-Nielsen, Methanation of CO over Nickel: Mechanism and Kinetics at High H_2/CO Ratios, J. Phys. Chem. B. 109(6) (2005) 2432–2438

[73] F. Aupretre, C. Descorme, D. Duprez, D. Casanave, D. Uzio, Ethanol steam reforming over $Mg_XNi_{1-X}Al_2O_3$ spinel oxide-supported Rh catalysts, J. Catal. 233(2) (2005) 464-477

[74] T. van Haasterecht, M. Swart, K.P. de Jong, J.H. Bitter, Effect of initial nickel particle size on stability of nickel catalysts for aqueous phase reforming, J. Energy Chem. 25(2) (2016) 289-296

[75] M. El Doukkali, A. Iriondo, J.F. Cambra, I. Gandarias, L. Jalowiecki-Duhamel, F. Dumeignil, P.L Arias, Deactivation study of the Pt and/or Ni-based γ-Al_2O_3 catalysts used in the aqueous phase reforming of glycerol for H_2 production, Appl. Catal. A:Gen. 472 (2014) 80–91

[76] A. Iriondo, J.F. Cambra, V.L. Barrio, M.B. Guemez, P.L. Arias, M.C. Sanchez-Sanchez, R.M. Navarro, J.L.G. Fierro, Glycerol liquid phase conversion over monometallic and bimetallic catalysts: Effect of metal, support type and reaction temperatures, Appl. Catal. B:Environ. 106(1–2) (2011) 83-93

FIGURE ANS SCHEME CAPTIONS

Figure 1. H_2-TPR profiles for (A) fresh samples; (B) catalysts used in APR reaction: NiAl-T-u: used for 2 h at 235 ºC/35 bar; NiAl-T-50 h: used for 50 h at 235 ºC/35 bar.

Figure 2. XRD spectra of the fresh samples (A) and spent catalysts (B).

Figure 3. DRS UV-vis NIR spectra of the samples, obtained at ambient temperature, and detailed spectra in the 500-800 nm region.

Figure 4. Chemical shift (A) and variation of chemical shift of Al_{Oh} with reduction temperature (B).

Figure 5. Surface acid sites density (A) and Surface basic sites density (B).

Figure 6. (A) Glycerol conversion, conversion to gas, hydrogen yield and selectivity to gas. (B) Specific hydrogen production rate. Reaction conditions: 250 ºC/45 bar (0.5 g of catalysts, feed rate 0.2 mL/min, 10 wt.% glycerol in water mixture, WHSV= 24.5 h^{-1}, data at steady state = 2 h).

Figure 7. Gas phase composition (dry basis) (in bars), and total gas flow (line).

Figure 8. (A) Molar composition of the main liquid products, and (B) mole distribution between products of dehydrogenation and dehydration/hydrogenation. Reaction conditions: 250 ºC/45 bar (0.5 g of catalysts, feed rate 0.2 mL/min, 10 wt.% glycerol in water mixture, WHSV= 24.5 h^{-1}, data at steady state = 2 h).

Figure 9. Effect of operation conditions (T/P) on the catalyst performance: (A) gas phase, and (B) liquid phase.

Figure 10. Evolution of X_{Gly} (blue), X_{gas} (grey) and S_{gas} (red) with TOS. Filled symbols: NiAl-850; Open symbols: NiAl-700. Reaction conditions: 235 ºC/35 bar (0.5 g of catalysts, feed rate 0.2 mL/min, 10 wt.% glycerol in water mixture, WHSV= 24.5 h^{-1}).

Figure 11. Variation of reaction indices with TOS. (A) NiAl-700; (B) NiAl-800; (C) Liquid phase indices.

Scheme 1. Reaction pathway proposed for the glycerol APR on nickel aluminate spinel-derived nickel catalysts.

FIGURE 1

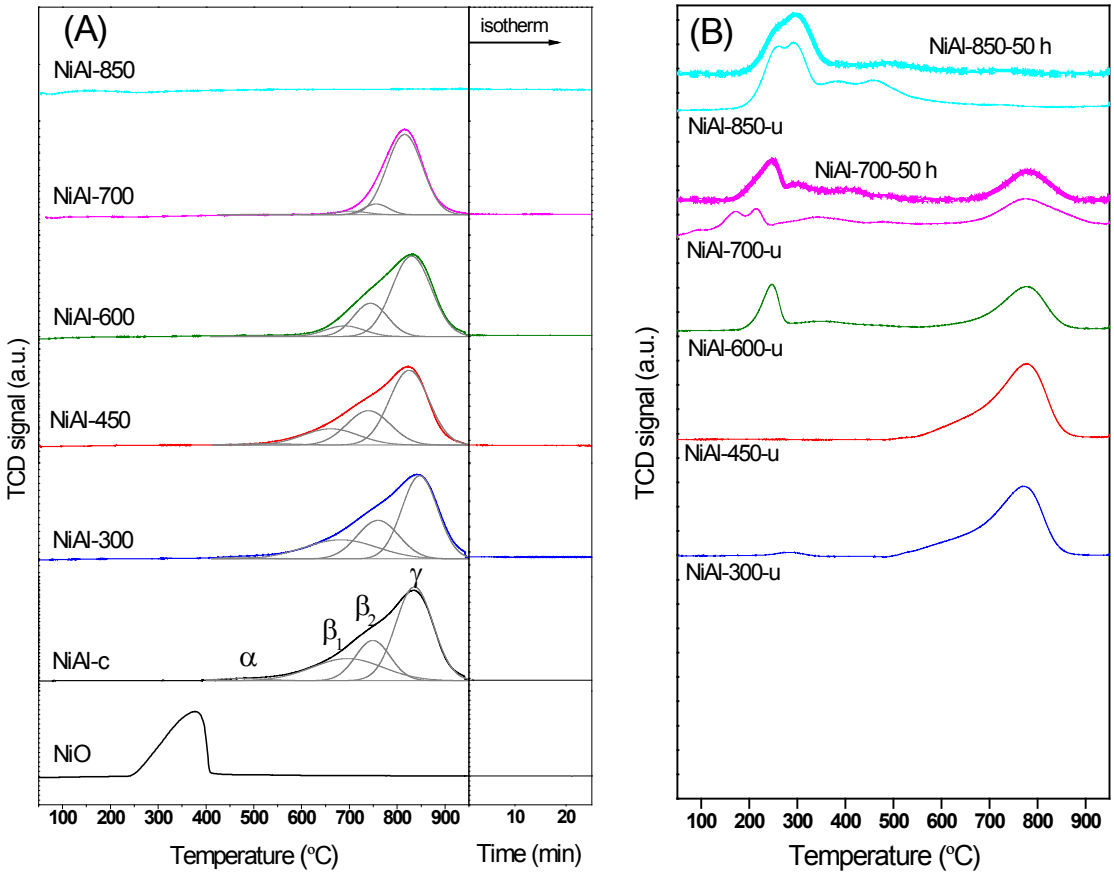

Fig. 1. H_2-TPR profiles for (A) fresh samples; (B) catalysts used in APR reaction: NiAl-T-u: used for 2 h at 235 °C/35 bar; NiAl-T-50 h: used for 50 h at 235 °C/35 bar.

FIGURE 2

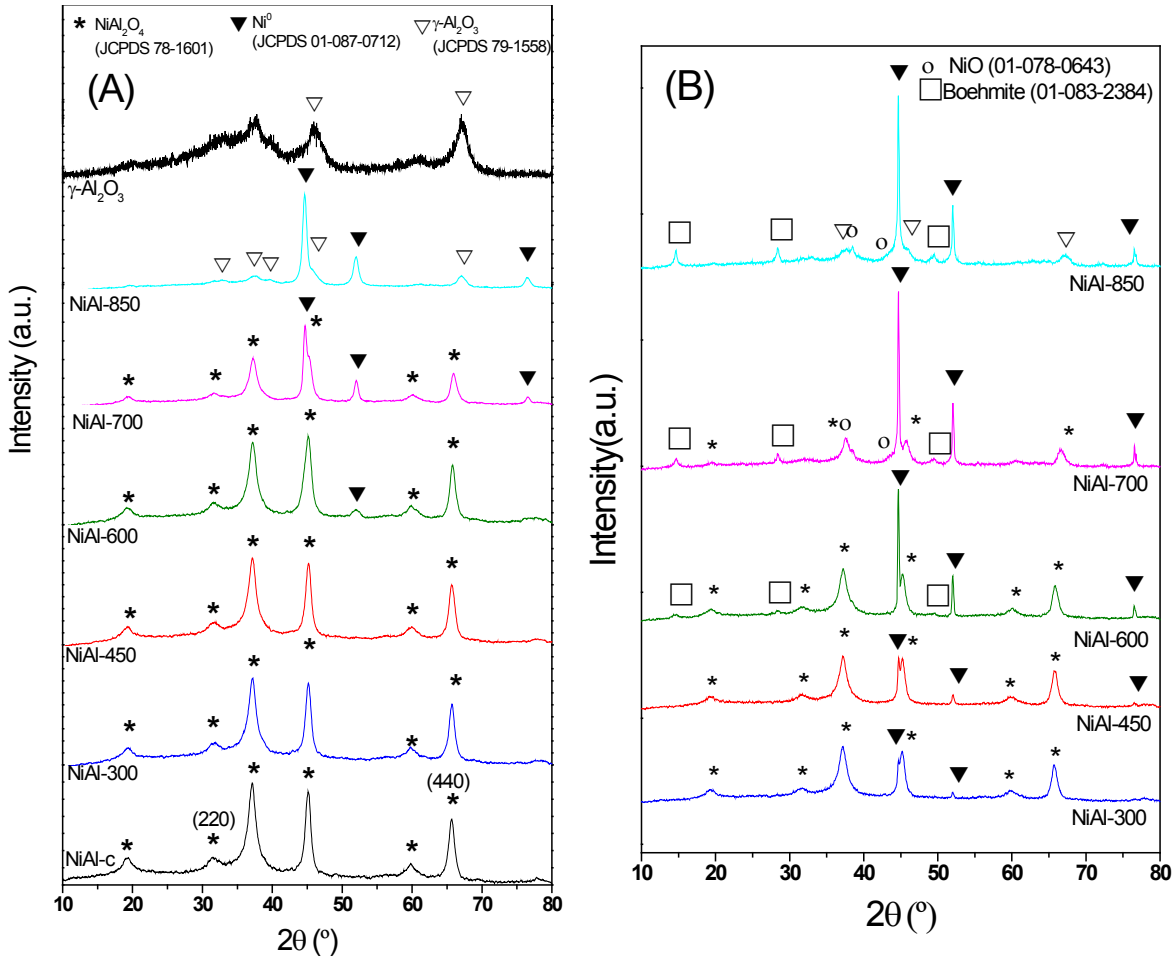

Fig. 2. XRD spectra of the fresh samples (A) and spent catalysts (B).

FIGURE 3

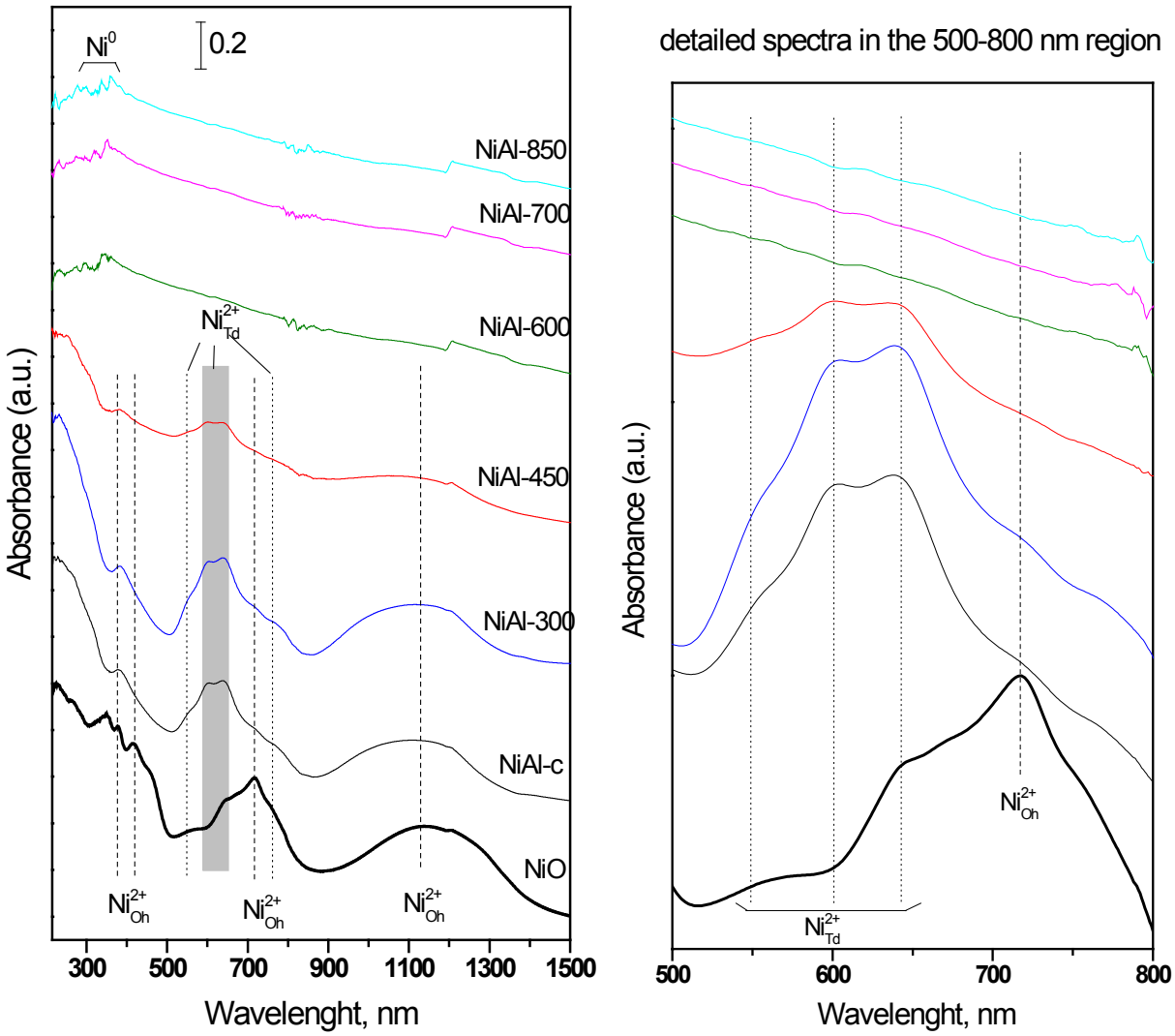

Fig. 3. DRS UV–vis NIR spectra of the samples, obtained at ambient temperature, and detailed spectra in the 500–800 nm region.

FIGURE 4

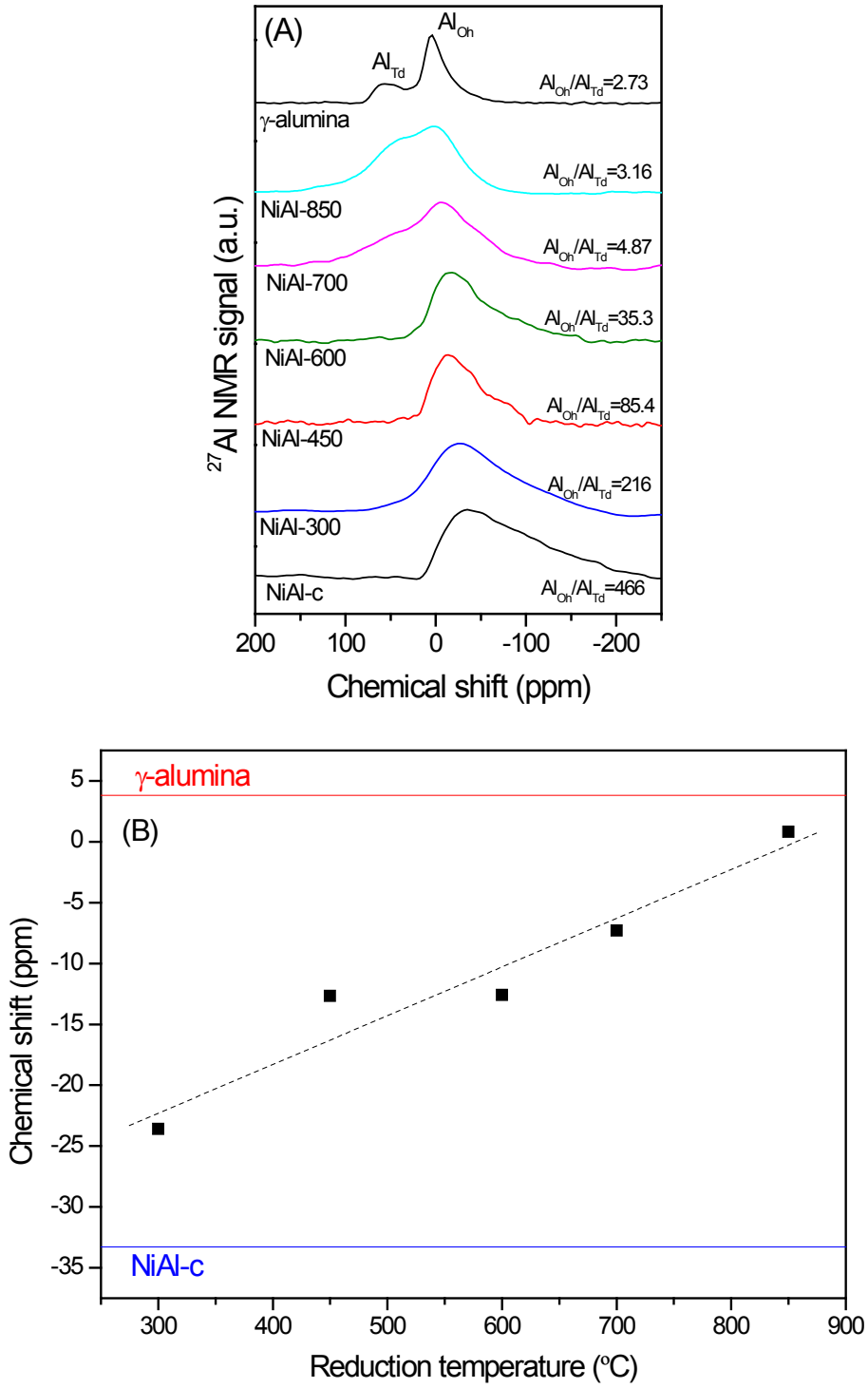

Fig. 4. Chemical shift (A) and variation of chemical shift of Al_{Oh} with reduction temperature (B).

FIGURE 5

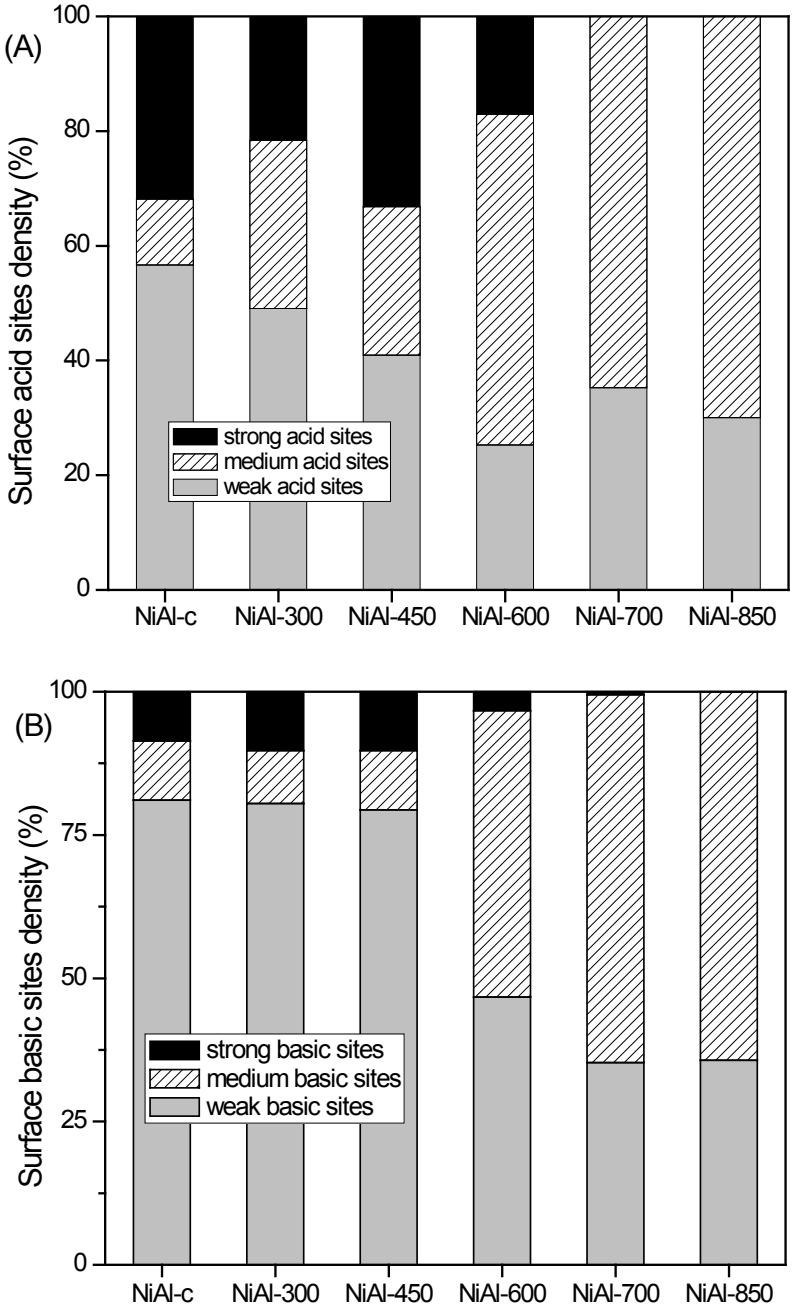

Fig. 5. Surface acid sites density (A) and Surface basic sites density (B).

FIGURE 6

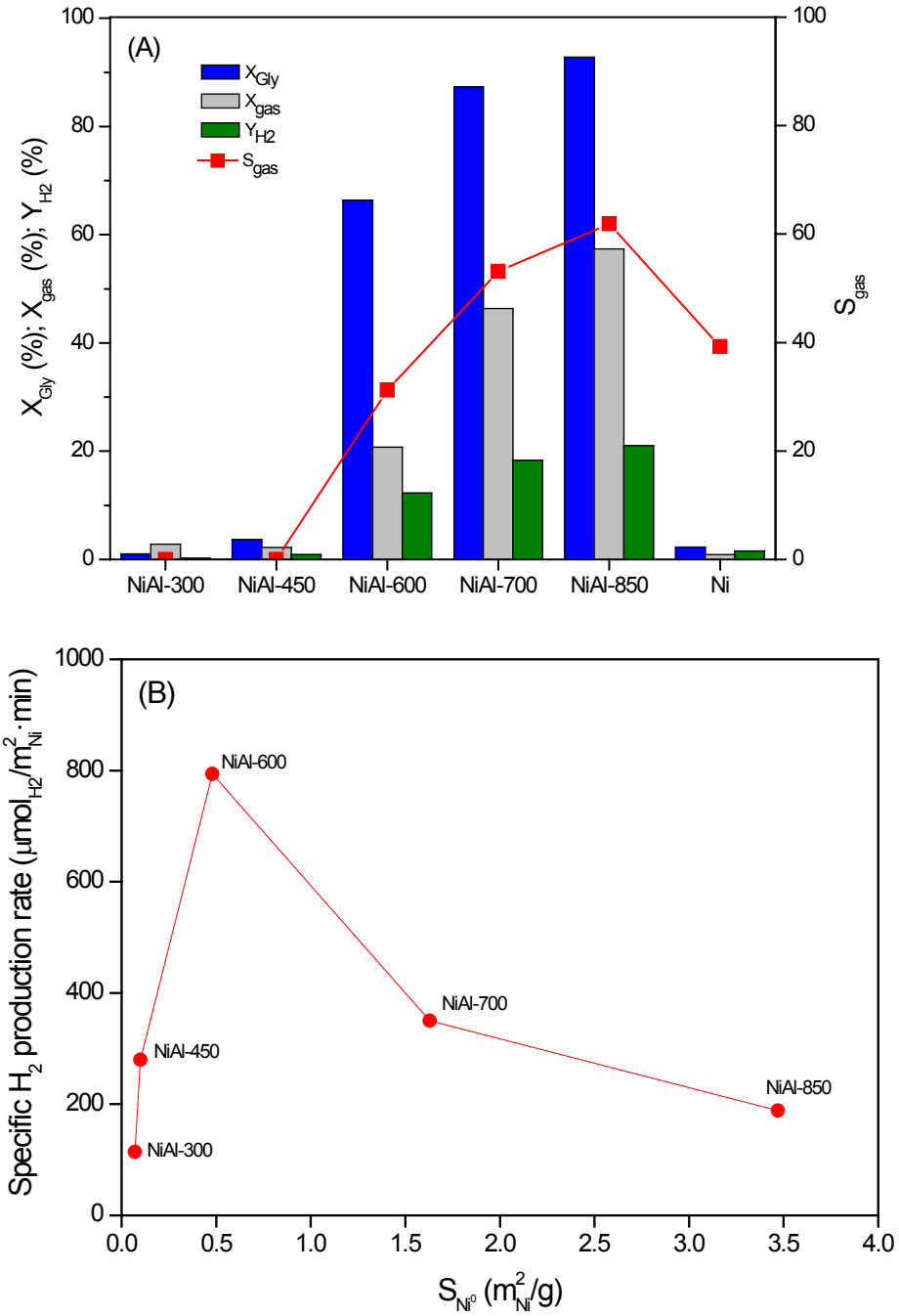

Fig. 6. (A) Glycerol conversion, conversion to gas, hydrogen yield and selectivity to gas. (B) Specific hydrogen production rate. Reaction conditions: 250 °C/45 bar (0.5 g of catalysts, feed rate 0.2 mL/min, 10 wt.% glycerol in water mixture, WHSV=24.5 h^{-1}, data at steady state=2 h).

FIGURE 7

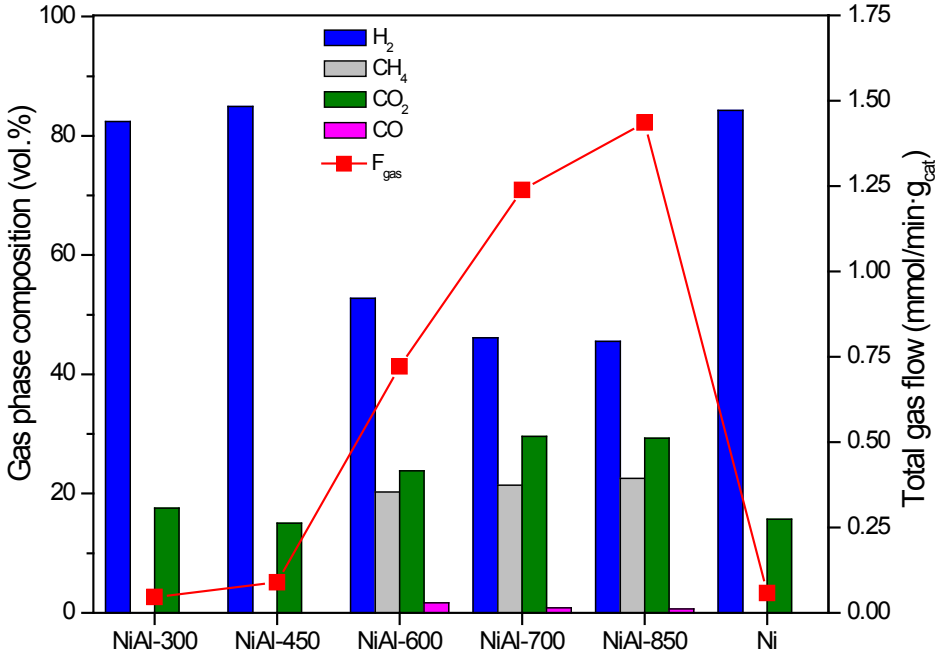

Fig. 7. Gas phase composition (dry basis) (in bars), and total gas flow (line).

FIGURE 8

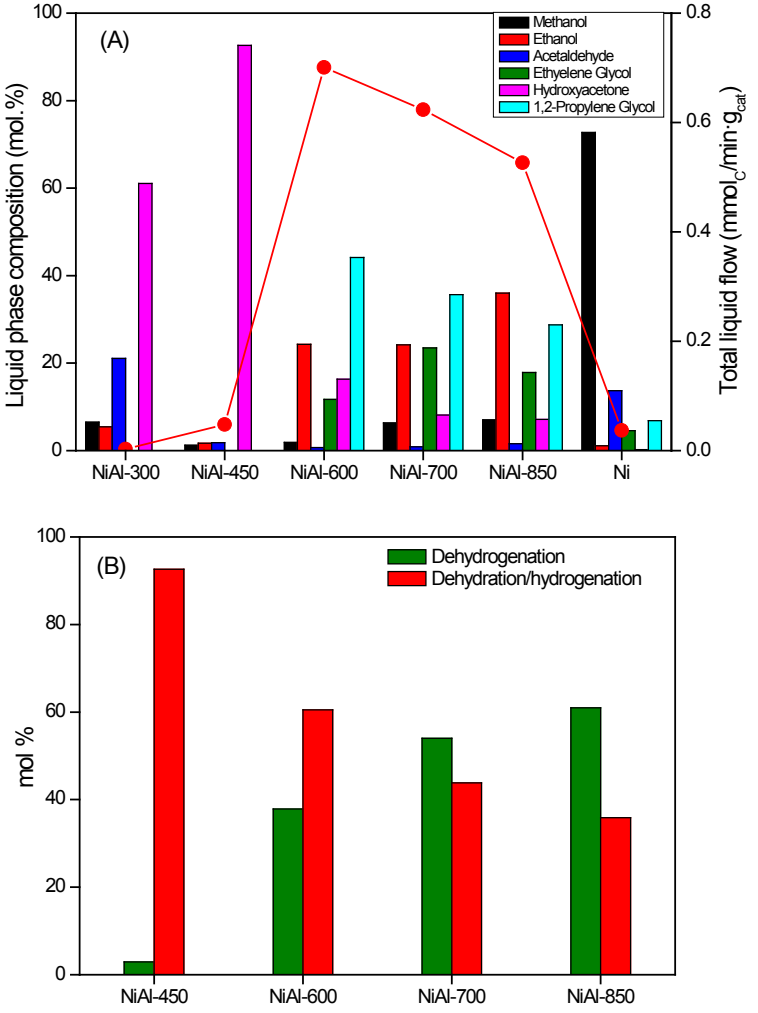

Fig. 8. (A) Molar composition of the main liquid products, and (B) mole distribution between products of dehydrogenation and dehydration/hydrogenation. Reaction conditions: 250 °C/45 bar (0.5 g of catalysts, feed rate 0.2 mL/ min, 10 wt.% glycerol in water mixture, WHSV=24.5 h^{-1}, data at steady state = 2 h).

FIGURE 9

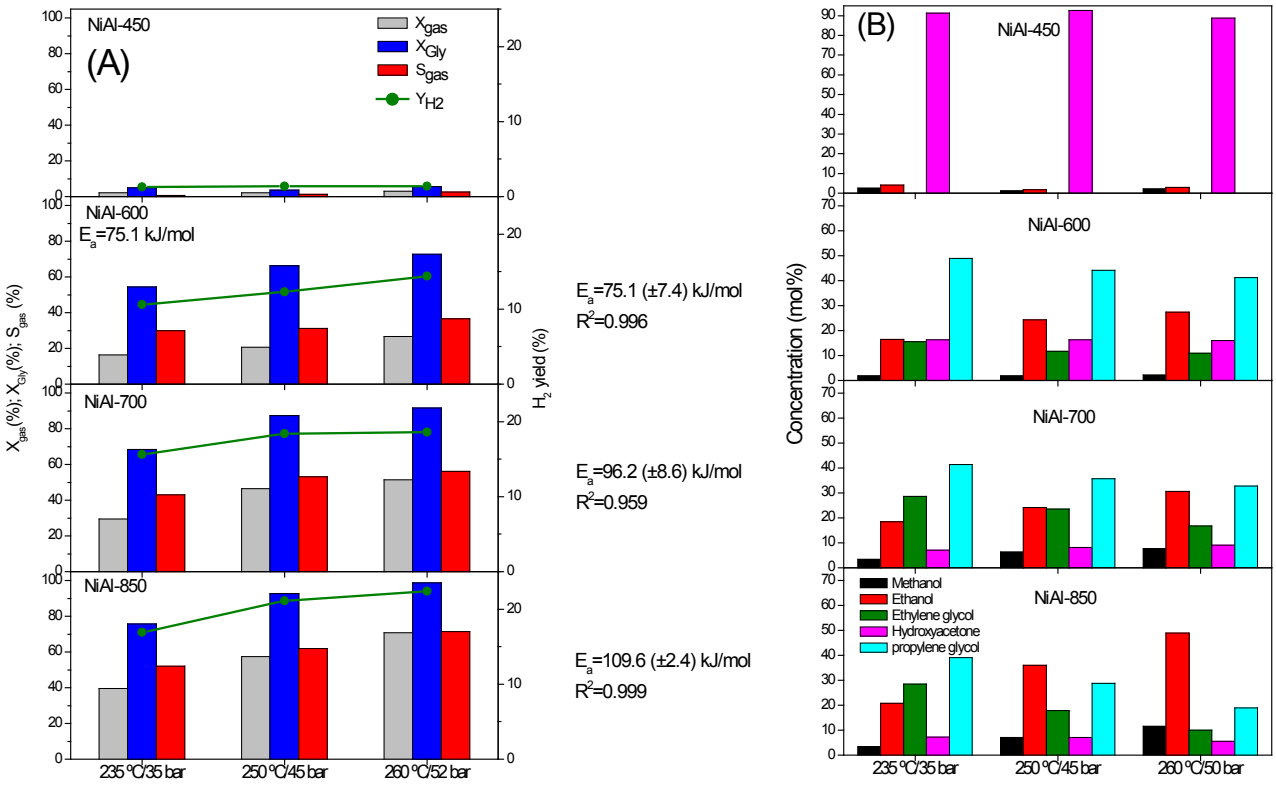

Fig. 9. Effect of operation conditions (T/P) on the catalyst performance: (A) gas phase, and (B) liquid phase.

FIGURE 10

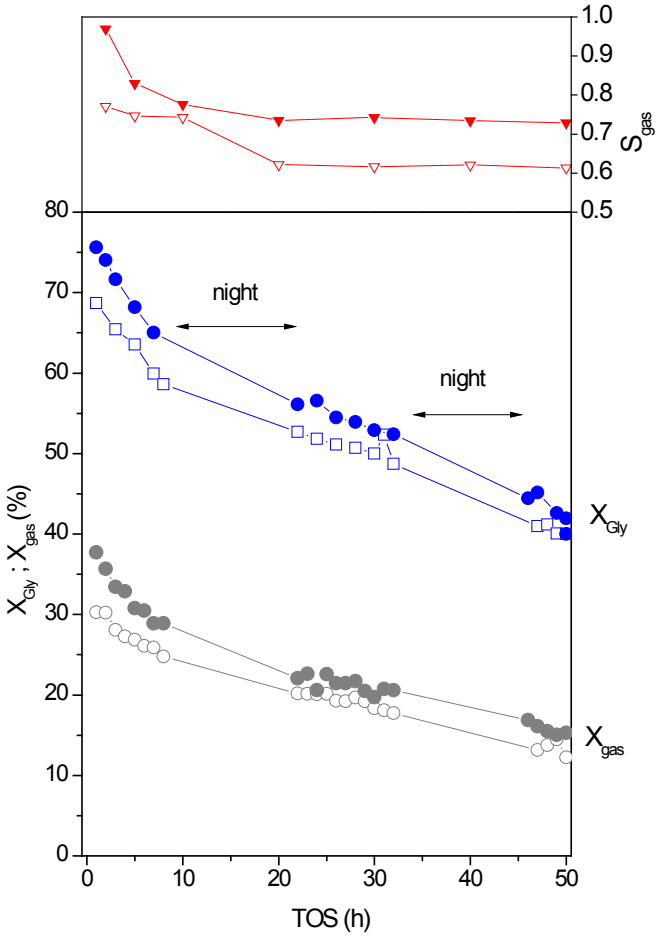

Fig. 10. Evolution of X_{Gly} (blue), X_{gas} (grey) and S_{gas} (red) with TOS. Filled symbols: NiAl-850; Open symbols: NiAl-700. Reaction conditions: 235 °C/35 bar (0.5 g of catalysts, feed rate 0.2 mL/min, 10 wt.% glycerol in wáter mixture, WHSV=24.5 h^{-1}) (For interpretation of the references to colour in this figure legend, the reader is referred to the web version of this article).

FIGURE 11

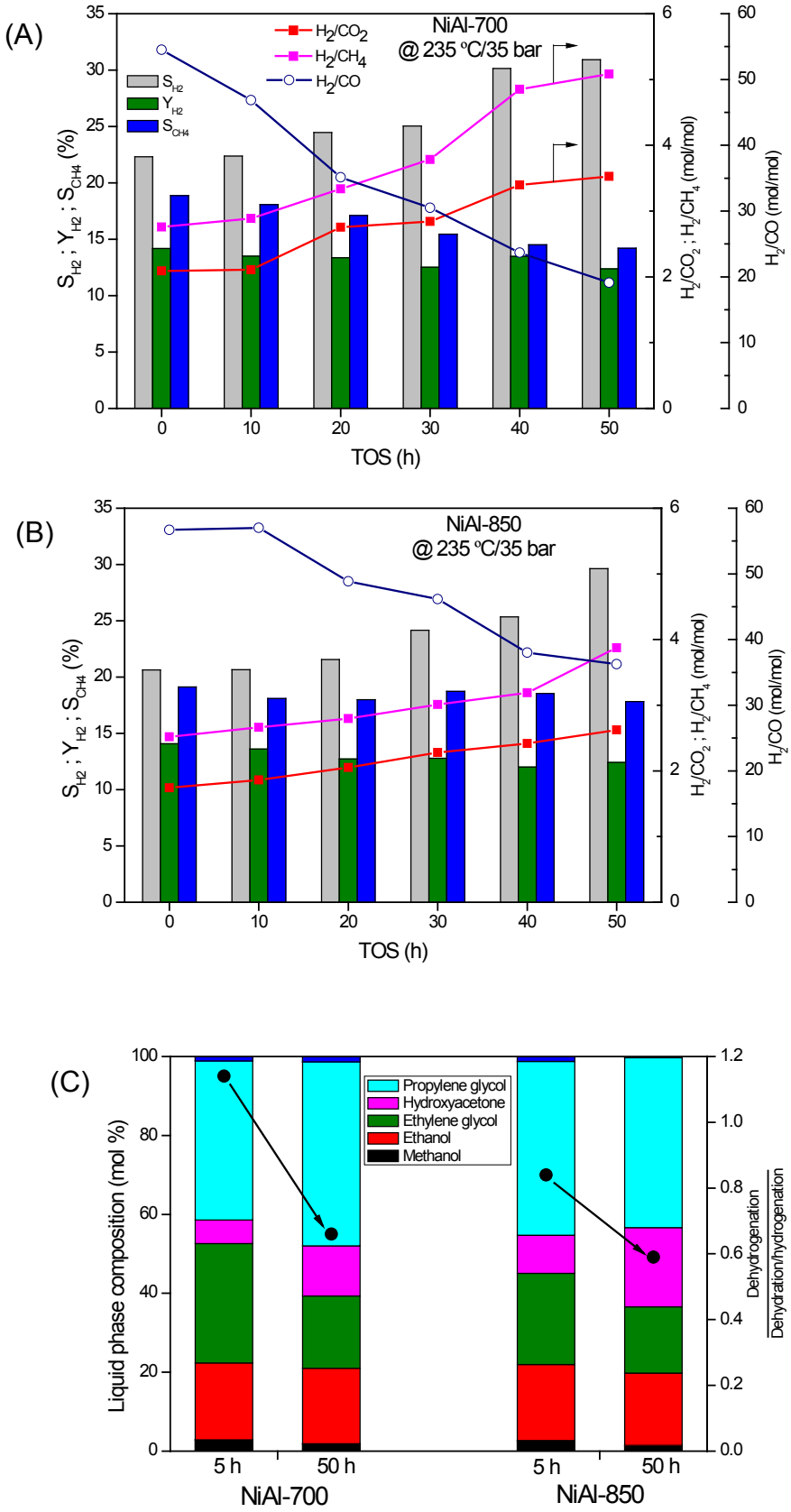

Fig. 11. Variation of reaction indices with TOS. (A) NiAl-700; (B) NiAl-800; (C) Liquid phase indices.

SCHEME 1

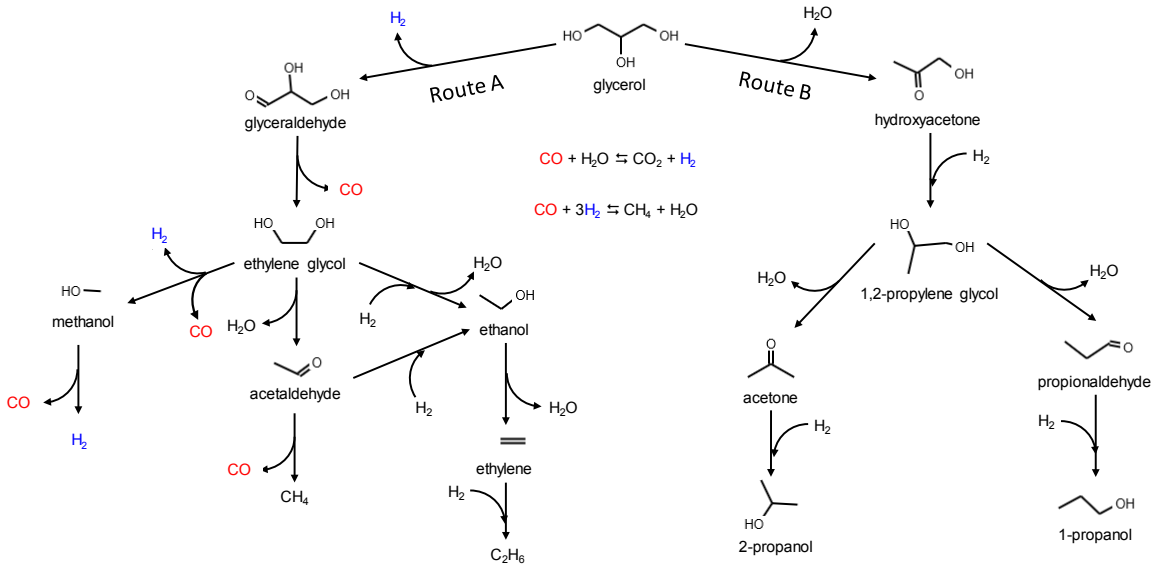

Scheme 1. Reaction pathway proposed for the glycerol APR on nickel aluminate spinel-derived nickel catalysts.

Table 1. Textural and structural characteristics of the fresh and spent catalysts.

Sample	Fresh samples							Spent samples						
	S_{BET} (m^2/g)	$d_{NiAl2O4}$ [a] (nm)	d_{Ni^0} [a] (nm)	Phases detected [a]	Acidity [b] $\mu mol_{NH3}/m^2$	Basicity [c] $\mu mol_{CO2}/m^2$	Acid/basic sites ratio	S_{BET} (m^2/g)	d_{Ni^0} [a] (nm)	$d_{boehmite}$ [a] (nm)	Phases detected [a]	Leached Ni [d] (%)	Leached Al [d] (%)	C [e] ($mmol_C/g$)
NiAl-c	98.0	8.9	n.d.	$NiAl_2O_4$	1.57	0.66	2.4	n.a.	n.a.	n.a.	n.a.	n.a.	n.a.	n.a.
NiAl-300	94.9	9.9	n.d.	$NiAl_2O_4$	1.57	0.59	2.7	102.6	33.9	n.d.	Ni^0 + $NiAl_2O_4$	0.65	<0.025	n.a.
NiAl-450	93.5	9.2	n.d.	$NiAl_2O_4$	1.93	0.39	4.9	87.0	30.0	n.d.	Ni^0 + $NiAl_2O_4$	0.78	<0.025	n.a.
NiAl-600	89.8	9.8	7.7	Ni^0 + $NiAl_2O_4$	1.82	0.73	2.3	110.2	45.9	8.1	Ni^0 + $NiAl_2O_4$ + boehmite	0.72	<0.025	n.a.
NiAl-700	83.1	9.1	13.6	Ni^0 + $NiAl_2O_4$	1.70	1.13	1.6	97.4 (92.6)	44.5 (32.0)	15.0 (7.7)	Ni^0 + $NiAl_2O_4$ + boehmite	0.27 (6.5)	<0.025 (<0.025)	(1.12)
NiAl-850	76.6	7.0*	11.6	Ni^0 + γ-alumina	2.13	1.03	2.0	109.9 (102.9)	41.5 (44.1)	17.4 (7.5)	Ni^0 + $NiAl_2O_4$ + boehmite	0.19 (5.4)	<0.025 (<0.025)	(0.16)

[a] from XRD. [b] from NH_3-TPD. [c] from CO_2-TPD. [d] from ICP-AES. [e] carbonaceous deposits by TPO-MS.

∗ γ-alumina

In parentheses, data for experiments with TOS 50 h

Table 2. Results from H_2-TPR and H_2 chemisorption of the calcined NiAl-c and fresh reduced NiAl-T and used catalysts (2 h TOS).

	Fresh samples									Used samples	
	H_2 consumption ($mmolH_2/g$)		$f_{Ni,red}$ (%)	Distribution of Ni (mmol Ni/g)					H_2 chemisorption	H_2-TPR	H_2 chemisorption
Sample	TPR-a	TPR-c		As Ni^0	As Surface NiO (peak α)	As $Ni_{1-X}Al_2O_{4-X}$ (peak β)	As $NiAl_2O_4$ (peak γ)	mole ratio β_1/β_2	Ni^0 area (m^2/g_{cat})	Oxidised Ni (%)	Ni^0 area (m^2/g_{cat})
NiAl-c	5.2	-	-	0 (0.0)	0.08 (1.5)	2.32 (44.7)	2.79 (53.8)	1.10	0	n.a.	n.a.
NiAl-300	-	5.0	3.8	0.20 (3.8)	0.10 (1.9)	2.32 (44.5)	2.59 (49.7)	0.90	0.07	< Q.L.	0.01
NiAl-450	-	4.9	5.8	0.30 (5.9)	n.d	2.19 (42.8)	2.63 (51.4)	0.72	0.10	< Q.L.	0.03
NiAl-600	-	4.1	21.1	1.10 (21.4)	n.d	1.30 (25.3)	2.74 (53.3)	0.47	0.48	124	0.06
NiAl-700	-	2.3	55.8	2.90 (56.2)	n.d	0.30 (5.8)	1.96 (38.0)	0.44	1.63	43 / 34*	0.08
NiAl-850	-	0.01	99.8	5.19 (99.8)	n.d	0 (0)	0.01 (0.2)	0	3.47	45 / 34*	0.23

In parentheses, as mole %
*, values for 50 h TOS
Q.L. Quantification level

Table 3. Comparison of the performance of nickel aluminate spinel-derives catalysts with other researches for APR of glycerol.

T (ºC)/ P (bar)	Reactor	Catalyst	Feed, WHSV or gly/cat	X_{Gly} (%)	X_{gas} (%)	S_{H2} (%)	Y_{H2} (%)	S_{gas} (%)	Ref.
250/50	Fixed-bed	Ni/Al_2O_3, CP, 5% Ni	10% gly/w, 2.45 h^{-1}	67	87	-	-	43	[49]
250/50	Fixed-bed	Ni/Al_2O_3, IMP, 10% Ni	10% gly/w, 2.6 h^{-1}	40	10	-	-	25	[9]
250/20	Fixed-bed	Ni/$LaAlO_3$, DP, 15% Ni	15% gly/w, 5.2 h^{-1}	23	-	61	-	-	[50]
240/40	Fixed-bed	Ni/CeO_2/Al_2O_3, IMP, 6% Ni, 3% CeO_2	1% gly/w, 12 h^{-1}	26	-	49	12	-	[51]
250/35	Fixed-bed	Ni/HTLC, CP, 20% Ni, Al/Al+Mg=0.24	10% gly/w, 5.1 h^{-1}	30	16	31	10	18	[13]
250/25	Fixed-bed	Ni/$Ce_{0.3}Zr_{0.7}O_2$, CP, 10% Ni	10% gly/w, 2.45 h^{-1}	90	99	-	-	37	[52]
225/28	Microreactor Fixed-bed	Pt-Re/AC, IMP, 3%Pt, 3%Re	10% gly/w, 5.0 h^{-1}	88	58	24.5	-	22	[53]
250/45	Batch	Pt-K/HT, IMP, 1%Pt, 2.8%K	10% gly/w gly/cat=0.1, t=4 h	88	87	-	48	33	[54]
225/27.6	Fixed bed	Pt/MgO, IMP, 0.79% Pt	5% gly/w, 3.6 h^{-1}	-	38	60	28	-	[55]
250/45	Fixed bed	$NiAl_2O_4$, CP, 33% Ni	10% gly/w, 24.5 h^{-1}	93	57	23	21	62	This work

gly/w: glycerol to water weight ratio in the feed, continuous reactor
gly/cat: glycerol to catalyst weight ratio in the feed, batch reactor
t: reaction time, batch reactor
HTLC: hydrotalcite-like compound
AC: activated carbon
IMP: impregnation
DP: deposition-precipitation
CP: coprecipitation

Table 4. Experimental results for the APR of 10 wt% glycerol at 250 ºC and 45 bar over NiAl-T catalysts for 2 h

Catalyst	S_{gas} (%)	S_{H2} (%)	S_{CH4} (%)	H_2/CO_2	CO/H_2	Y_{H2} (%)	S_{C2} (%)	S_{C3} (%)
NiAl-300	~0	95	0	4.7	0	0.7	0	0
NiAl-450	~0	90	0	5.6	0	1.4	0	4.95
NiAl-600	31.2	18	17	2.2	0.032	12.3	0.44	0.23
NiAl-700	53.1	21	23	1.6	0.018	18.4	0.47	0.27
NiAl-850	61.9	23	26	1.6	0.015	21.1	0.43	0.23
Ni	39.1	56	0	5.4	0.00	1.58	0	0

NICKEL ALUMINATE SPINEL-DERIVED CATALYSTS FOR THE AQUEOUS PHASE REFORMING OF GLYCEROL: EFFECT OF REDUCTION TEMPERATURE

A. Morales-Marín[1], J.L. Ayastuy[1,*], U. Iriarte-Velasco[2], M.A. Gutiérrez-Ortiz[1]

SUPPORTING INFORMATION

*Corresponding author: joseluis.ayastuy@ehu.eus

1. Textural characterization

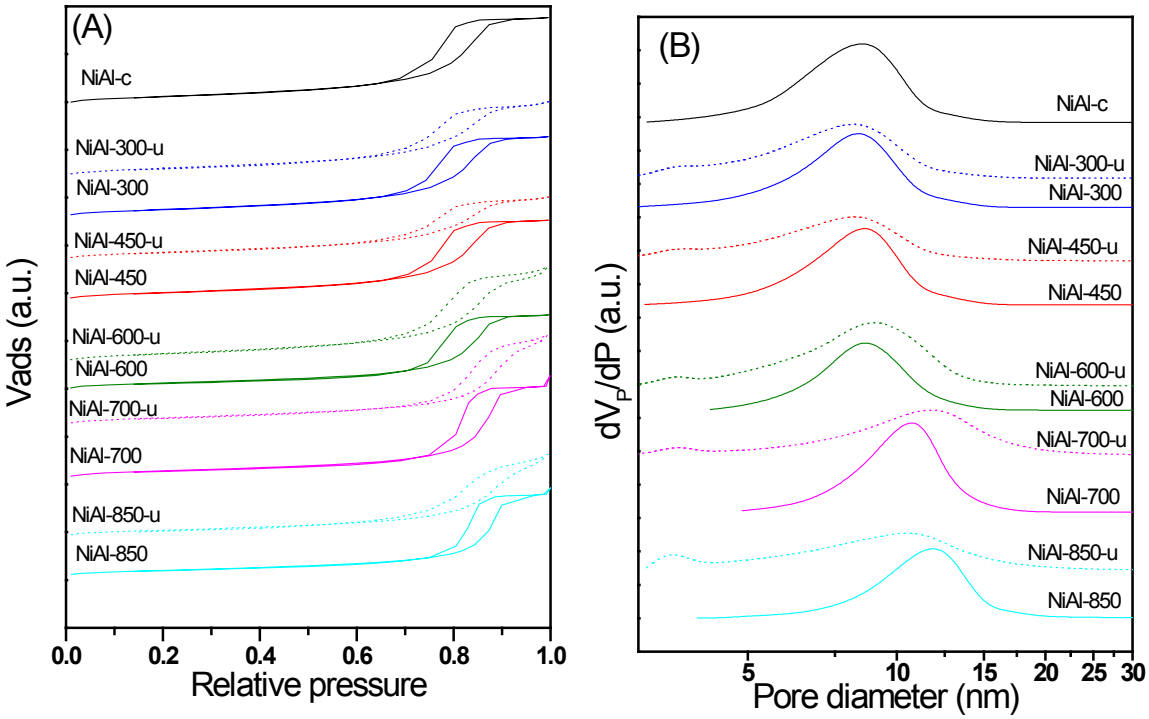

Figure S1. N_2 physisorption isotherms (A) and pores size distribution (B) for fresh (NiAl-T) and used (NiAl-T-u) samples.

Table S1. Textural properties of the fresh and used (2 h TOS) catalysts.

Sample	Fresh samples		Used samples	
	V_P (cm^3/g)	d_P (nm)	V_P (cm^3/g)	d_P (nm)
γ-alumina	0.13	3.6	-	-
NiAl-c	0.27	8.4	-	-
NiAl-300	0.27	8.3	0.27	7.9
NiAl-450	0.28	8.4	0.22	7.7
NiAl-600	0.28	9.1	0.33	9.1
NiAl-700	0.29	10.8	0.33	10.6
NiAl-850	0.29	11.8	0.31	8.3

2. Structural characterization

The unit cell parameters of the nickel-containing phases identified by XRD ($NiAl_2O_4$ and Ni^0) were also calculated from the XRD diffractograms (Table S3). Spinel crystallized into *Fd-3m* cubic system (JCPDS 00-010-0339) while metallic nickel crystallized ordinarily into *Fm-3m* cubic system (JCPDS 01-087-0712). Exposition to hydrogen atmosphere notably decreased the unit cell parameter of the nickel aluminate spinel, more pronounced with the increase of the reduction temperature (from 0.8044 nm for NiAl-c to 0.8010 nm for NiAl-700). According to Halevy et al. [1] this could be explained in terms of the compressive residual stresses generated during reduction of the mixed oxide.

The unit cell parameter of the metallic nickel was almost unaffected (around 0.352 nm) independent of the reduction temperature, which suggested that metallic nickel phase was not transformed, for example, into a quite unusual hexagonal close packed phase [2].

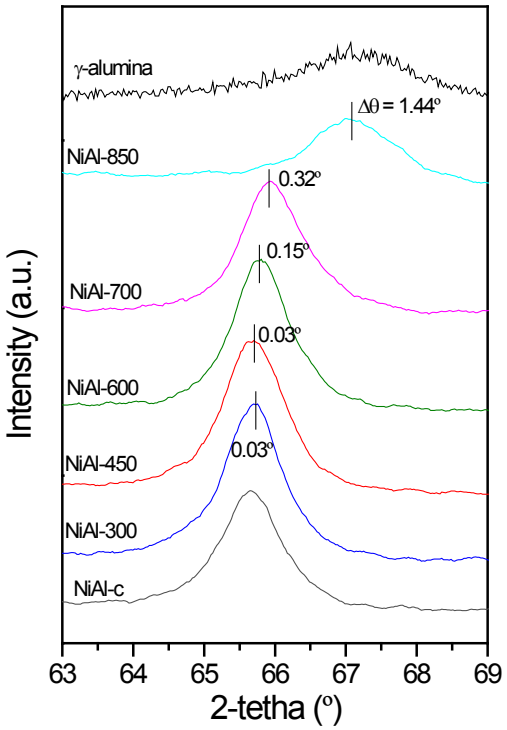

Figure S2. Shift of the peak at 65º with reduction temperature with respect to (440) plane of NiAl-c.

Figure S3A shows the IR skeletal spectra of the fresh NiAl samples. The spectra for NiO and γ-alumina have also been included for comparison purposes. For NiO, a broad band at 400-700 cm^{-1} corresponding to the vibration of Ni-O bond was observed revealing the presence of NiO nanocrystals [3]. IR bands related to the physically absorbed water were almost unappreciable, due to the low water adsorption capacity of NiO as a consequence of its very low surface (S_{BET}=0.1 m^2/g). For γ-alumina the broad peak at around 3410 cm^{-1} (with three defined peaks at 3415, 3454 and 3542 cm^{-1})

was due to the presence of surface hydroxyl groups (OH stretching–Al–OH) and peaks at 1619 and 1637 cm^{-1} were due to OH^- bending. The absorption bands below 1000 cm^{-1} corresponded to the vibrational modes of coordinated aluminum oxides i.e. bending modes of O-Al-O (484 cm^{-1}) and stretching modes of Al-O-Al (607 cm^{-1}) [4]. Substantial differences were found in the spectrum of NiAl-c sample, in comparison to NiO. Similarly to γ-alumina, the broad band at 3422 cm^{-1} was assigned to the O-H stretching mode of water, while bands at 1382, 1505 and 1638 cm^{-1} were related to the vibration mode of the adsorbed water (not shown) [5].

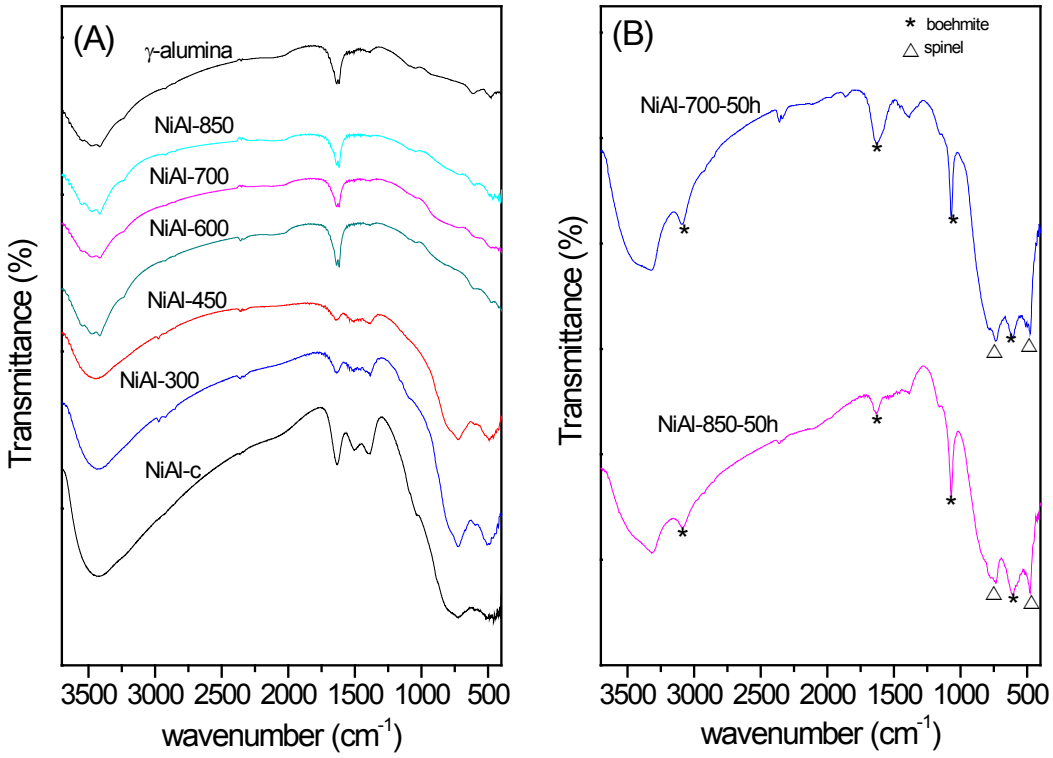

Figure S3. FTIR spectra of fresh catalysts (A) and spent catalysts (B).

The intense bands at 725 cm^{-1} and 492 cm^{-1} observed for NiAl-c are characteristic of spinel structure [6,7]. The broad bands at about 3420 cm^{-1} can be attributed to hydroxyl stretching and the bands at 1631, 1498 and 1385 cm^{-1} are due to OH bending [6]. The FTIR spectra significantly varied with reduction temperature. For instance, the bands characteristic for spinel remained for catalysts treated at low temperature (NiAl-300 and NiAl-450). Upon treatment above 600 ºC these bands disappeared and characteristic features of γ-alumina could be observed (484 cm^{-1} O-Al-O bending mode, 607 cm^{-1} Al-O-Al stretching mode) and a single OH bending at 1631 cm^{-1} [4]. It could be concluded that NiAl-c mainly contained nickel aluminate phase, which was readily transformed into γ-alumina under H_2 flow at 600 ºC.

FTIR spectra of catalysts NiAl-700 and NiAl-850 used for 50 h TOS (Figure S3(B)) revealed the existence of boehmite (611, 1068, 3089 cm^{-1}) [8].

Table S2. Structural parameters of the fresh catalysts.

Sample	$a_{NiAl2O4}$ [a] (Å)	a_{Ni^0} [a] (Å)	I_{220}/I_{440} [a]	$Ni^{2+}_{Td}/Ni^{2+}_{Oh}$ [b]	Exposed Ni^0 (at_{Ni^0}/g_{cat})
NiAl-c	8.044 ±0.0063	n.d.	0.25	1.44	0
NiAl-300	8.040 ±0.0060	n.d.	0.25	1.35	$1.14 \cdot 10^{18}$
NiAl-450	8.036 ±0.0088	n.d.	0.24	1.31	$1.53 \cdot 10^{18}$
NiAl-600	8.028 ±0.0053	3.520 ±0.0026	0.22	n.d.	$7.37 \cdot 10^{18}$
NiAl-700	8.010 ±0.0061	3.519 ±0.0032	0.21	n.d.	$25.1 \cdot 10^{18}$
NiAl-850	7.879 [c]	3.522 ±0.0021	n.d.	n.d.	$53.4 \cdot 10^{18}$

[a] from XRD. [b] from DRS UV-vis NIR.

3. Acidity-basicity

Temperature programmed desorption (Figure S4) was used to characterize the acid and basic strength distribution, assuming that the desorption temperature could be related to the strength of acid and basic sites. In NH_3-TPD, the peaks observed in the low (below 250 ºC), medium (250-500 ºC) and high temperature (above 500 ºC) regions corresponds to weak, medium and strong acid sites, respectively.

Three temperature intervals were considered in CO_2-TPD: <150 ºC, ascribed to the weak basic sites (decomposition of bicarbonates on surface hydroxyl groups); 150-350 ºC, related to the medium strength basic sites (decomposition of bidentate carbonates species); and >350 ºC due to the strong basic sites, which are due to the decomposition of the unidentate carbonates species) [9]. Moreover, the unidentate and bidentate carbonates are formed on surface oxygen atoms of different coordination degree (unidentate over oxygen ions showing the lowest coordination number, bidentate over adjacent cationic site [10].

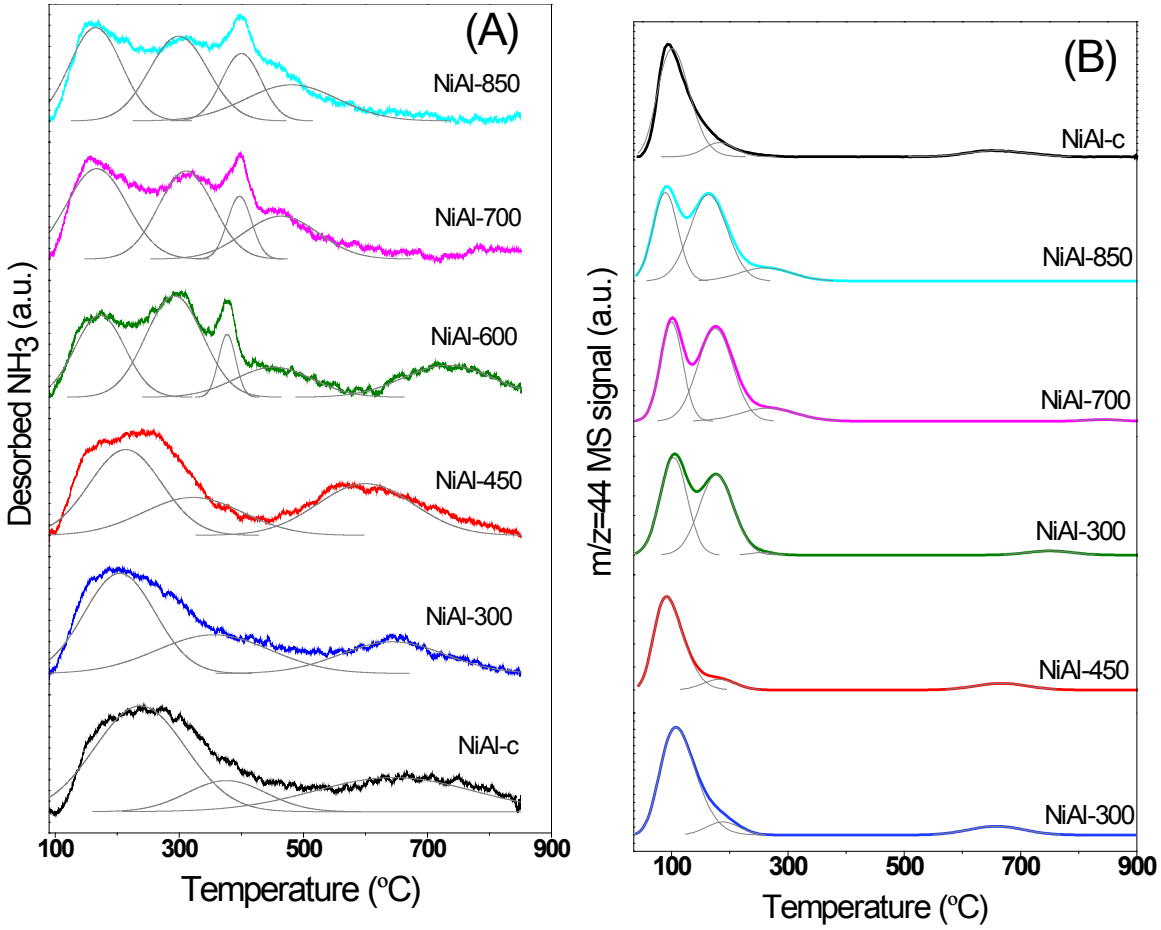

Figure S4. (A) NH_3-TPD and (B) CO_2-TPD profiles for NiAl-T catalysts.

4. Catalytic performance: Effect of working Temperature/Pressure conditions

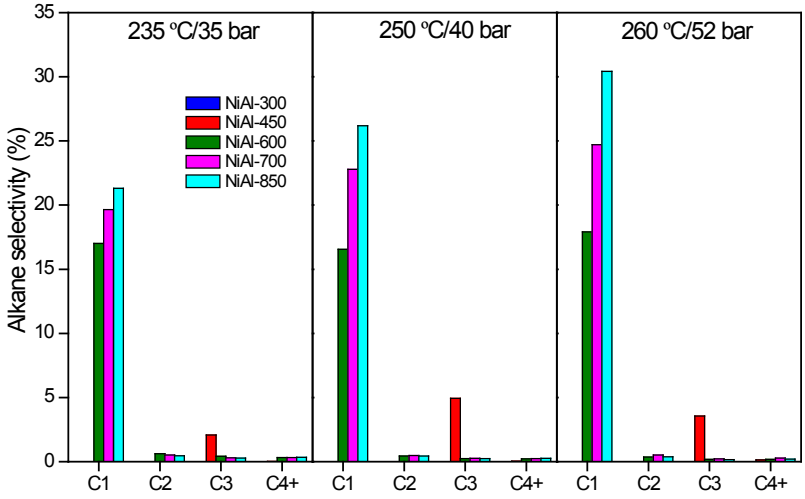

Figure S5. Alkane selectivity in function of C numbers.

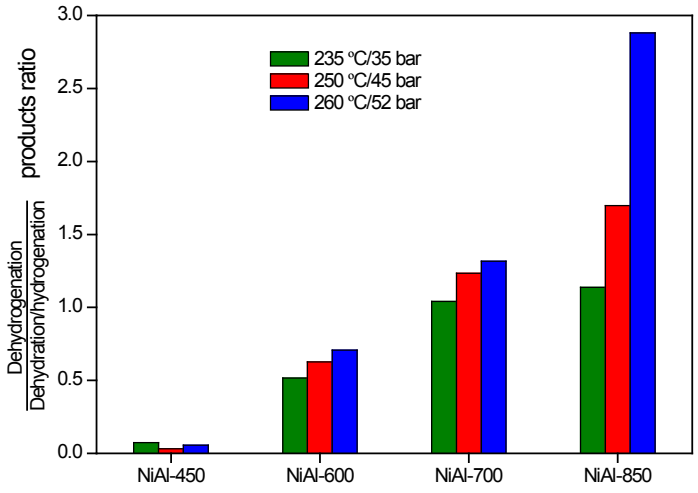

Figure S6. Route A/route B products for different T/P conditions.

Table S3. Gas phase composition, selectivities and hydrogen yield for different T/P operation conditions.

Catalyst	T (ºC)/ P (bar)	H_2 (%)	CH_4 (%)	S_{gas} (%)	S_{H2} (%)	S_{CH4} (%)	H_2/CO_2	CO/H_2	Y_{H2} (%)
NiAl-300	235/35	90.0	0.1	0	n.a.	n.a.	n.a	0.00	n.a.
	250/45	82.4	0.1	0	95	0	4.7	0.00	0.7
	260/50	82.4	0.1	6.0	98	0	4.8	0.00	0.9
NiAl-450	235/35	85.0	0.1	0	87	0	5.9	0.00	1.3
	250/45	85.0	0.2	0	90	0	5.6	0.00	1.4
	260/50	78.0	0.1	11.1	93	0	3.9	0.00	1.4
NiAl-600	235/35	54.2	20.4	30.0	19	17	2.5	0.03	10.6
	250/45	52.7	20.3	31.2	18	17	2.2	0.03	12.3
	260/50	51.8	20.2	36.5	20	18	2.1	0.04	14.4
NiAl-700	235/35	52.5	18.4	43.1	23	20	2.1	0.02	15.6
	250/45	46.1	21.4	53.1	21	23	1.6	0.02	18.4
	260/50	45.0	23.5	56.2	20	25	1.6	0.02	18.6
NiAl-850	235/35	48.0	19.7	52.1	22	21	1.6	0.02	16.9
	250/45	45.6	22.5	61.9	23	26	1.6	0.02	21.1
	260/50	43.4	25.0	71.5	23	30	1.5	0.01	22.4
Ni	235/35	73.5	0.1	42.0	93	0	2.8	0.00	2.1
	250/45	84.3	0.2	39.1	56	0	5.4	0.00	1.6
	260/50	90.4	0.1	48.0	50	0	9.4	0.00	1.8

5. H_2-TPR of the spent catalysts

Table S4. TPR data for catalysts used in glycerol APR (2 h TOS at 250 ºC/45 bar).

Catalyst	H_2 consumption ($mmol_{H2}/g$)			
	Total	Interval 50 - 600 ºC	Interval 600 - 750 ºC	> 750 ºC
NiAl-300	4.46	0.12	1.92	2.42
NiAl-450	4.49	0.03	1.89	2.57
NiAl-600	3.33	1.36	0.43	1.54
NiAl-700	2.41 (1.85)	1.24 (0.99)	0.12 (0.26)	1.05 (0.60)
NiAl-850	2.56 (1.89)	2.34 (1.78)	0.22 (0.11)	n.d. (n.d.)

In parenthesis, data for catalysts used during 50 h (TOS)

6. References Supported Material

[1] I. Halevy, D. Dragoi, E. Üstündag, A.F. Yue, E.H. Arredondo, J. Hu, M.S. Somayazulu, The effect of pressure on the structure of $NiAl_2O_4$, J. Phys. Condens. Matter. 14(44) (2002) 10511–10516

[2] G. Carturan, S. Enzo, R. Ganzerla, M. Lenarda, R. Zanoni, Role of solid-state structure in propene hydrogenation with nickel catalysts , J. Chem. Soc. Faraday Trans. 86(4) (1990) 739-746

[3] P. Gogoi, B.J. Saikia, S.K. Dolui, Effects of Nickel Oxide (NiO) nanoparticles on the performance characteristics of the jatropha oil based alkyd and epoxy blends, J. Appl. Polym. Sci. 132(8) (2015) 41490-41498

[4] J. Gangwar, B.K. Gupta, S.K. Tripathi, A.K. Srivastava, Phase dependent thermal and spectroscopic responses of Al_2O_3 nanostructures with different morphogenesis, Nanoscale 7 (2015) 13313-13344

[5] Y. Absalan, I.G. Bratchikova, N.N. Lobanovc, O.V. Kovalchukova, Novel synthesis method for photo-catalytic system based on some 3d-metal titanates, J. Mater. Sci: Mater. Electron. 28(23) (2017) 18207–18219

[6] N. Bayal, P. Jeevanandam, Synthesis of metal aluminate nanoparticles by sol–gel method and studies on their reactivity, J. Alloys Compd. 516 (2012) 27-32

[7] E. Leal, A.C.F.M. Costa, N.L. de Freita, H.L. Lira, R.H.G.A. Kiminami, L. Gama, $NiAl_2O_4$ catalysts prepared by combustion reaction using glycine as fuel, Mater. Res. Bull. 46(9) (2011) 1409–1413

[8] A.B. Kiss, G. Keresztury, L. Farkas, Raman and i.r. spectra and structure of boehmite (γ-AlOOH). Evidence for the recently discarded D172h space group, Spectrochim. Acta Part A 36 (1980) 653–658

[9] Q. Liu, L. Wang, C. Wang, W. Qu, Z. Tian, H. Ma, D. Wang, B. Wang, Z. Xu, The effect of lanthanum doping on activity of Zn-Al spinel for transesterification, Appl. Catal. B:Environ. 136–137 (2013) 210– 217

[10] M. León, E. Díaz, S. Bennici, A. Vega, S. Ordóñez, A. Auroux, Adsorption of CO_2 on Hydrotalcite-Derived Mixed Oxides: Sorption Mechanisms and Consequences for Adsorption Irreversibility, Ind. Eng. Chem. Res. 49(8) (2010) 3663–3671